

Comprehensive Summaries of Uppsala Dissertations
from the Faculty of Science and Technology 859



Modelling Chemical Reactions

*Theoretical Investigations of Organic
Rearrangement Reactions*

BY

PER-ERIK LARSSON



ACTA UNIVERSITATIS UPSALIENSIS
UPPSALA 2003

Dissertation presented at Uppsala University to be publicly examined in Högssalen, Ångströmlaboratoriet, Uppsala, Friday, June 6, 2003 at 10:15 for the degree of Doctor of Philosophy. The examination will be conducted in English.

Abstract

Larsson, P-E. 2003. Modelling Chemical Reactions. Theoretical Investigations of Organic Rearrangement Reactions. Acta Universitatis Upsaliensis. *Comprehensive Summaries of Uppsala Dissertations from the Faculty of Science and Technology* 859. Uppsala. ISBN 91-554-5669-3

Chemical reactions are ubiquitous and very important for life and many other processes taking place on earth. In both theoretical and experimental studies of reactivity a transition state is often used to rationalise the outcome of such studies. The present thesis deals with calculations of transition states in radical cation rearrangements, and a principle of least motion study of the rearrangements in the barbaralyl cation.

In particular, alternative quadricyclane radical cation (Q^+) rearrangements are extensively studied. The rearrangement of Q^+ to norbornadiene is extremely facile and is often used as a prototype for one-electron oxidations. However, electron spin resonance (ESR) experiments show that there are additional cations formed from Q^+ . Two plausible paths for the rearrangement of Q^+ to the 1,3,5-cycloheptatriene radical cation are located. The most favourable one is a multistep rearrangement with two shallow intermediates, which has a rate-limiting step of 16.5 kcal/mol. In addition, a special structure, the bicyclo[2.2.1]hepta-2-ene-5-yl-7-ylum radical cation, is identified on these alternative paths; and its computed ESR parameters agree excellently with the experimental spectrum assigned to another intermediate on this path. Moreover, this cation show a homoconjugative stabilization, which is uncommon for radical cations.

The bicyclopopylidene (**BCP**) radical cation undergoes ring opening to the tetramethyleneethane radical cation upon γ -irradiation of the neutral **BCP**. This rearrangement proceeds through a stepwise mechanism for the first ring opening with a 7.3 kcal/mol activation energy, while the second ring opening has no activation energy. The dominating reaction coordinate during each ring opening is an olefinic carbon rehybridization.

The principle of least motion is based on the idea that, on passing from reactant to product, the reaction path with the least nuclear change is the most likely. By using hyperspherical coordinates to define a distance measure between conformations on a potential energy surface, a possibility to interpret reaction paths in terms of distance arises. In applying this measure to the complex rearrangements of the barbaralyl cation, a correct ordering of the conformations on this surface is found.

Per-Erik Larsson, Department of Quantum Chemistry, Box 518, Uppsala University, SE-75120 Uppsala, Sweden

© Per-Erik Larsson 2003

ISSN 1104-232X

ISBN 91-554-5669-3

urn:nbn:se:uu:diva-3475 (<http://urn.kb.se/resolve?urn=urn:nbn:se:uu:diva-3475>)

List of papers

This thesis is based on the following papers. Reprints were made with permission from the publishers.

I. Quadricyclane Radical Cation Rearrangements: A Computational study of the Transformations to 1,3,5-Cycloheptatriene and Norbornadiene

Larsson, P.-E.; Salhi-Benachenhou, N.; Lunell, S.

Submitted to Chem. Eur. J.

II. Bicyclo[2.2.1]hepta-2-ene-5-yl-7-ylum Radical Cation: A Theoretical Validation of a Bishomoaromatic Radical Cation Intermediate

Larsson, P.-E.; Salhi-Benachenhou, N.; Lunell, S.

Org. Lett. **5**, 1329 (2003).

III. Quadricyclane Radical Cation Isomerization Reactions: A Theoretical Study

Larsson, P.-E.; Salhi-Benachenhou, N.; Dong, X.; Lunell, S.

Int. J. Quant. Chem. **90**, 1388 (2002).

IV. Bicyclopropylidene Radical Cation: A Rehybridization Ring Opening to Tetramethyleneethane

Norberg, D.; Larsson, P.-E.; Dong, X.-C.; Salhi-Benachenhou, N.; Lunell, S.

Submitted to J. Am. Chem. Soc.

V. Topology and Least Motion. A Study of the Barbaralyl Cation

Larsson, P.-E.; Linderberg, J.

Theor. Chim. Acta **93**, 79 (1996).

Contents

List of papers	i
Contents	ii
1. Introduction.....	1
2. Chemical Models	2
A. From Quantum Mechanics to Quantum Chemistry.....	3
B. Potential Energy Surface	4
Born-Oppenheimer Separation.....	5
C. Concepts for Chemical Reactions.....	7
3. Quantum Chemistry	10
A. Methods.....	11
Hartree-Fock.....	11
Post Hartree-Fock.....	11
Density Functional Theory	13
B. Basis sets	15
C. Spin Density and Hyperfine Coupling Constants.....	16
4. Radical Cation Rearrangements.....	17
A. Quadricyclane Rearrangements to 1,3,5-Cycloheptatriene and Norbornadiene.....	17
Multistep Rearrangement	20
Bicyclo[2.2.1]hepta-2-ene-5-yl-7-ylum radical cation	23
B. Bicyclopropylidene: a Rehybridization Ring Opening to Tetramethyleneethane	25
Rehybridization Mechanism.....	28
5. Principle of Least Motion	30
A. Rice-Teller Measure	32
B. An Example: the Barbaralyl Cation.....	35
Acknowledgment.....	40
References.....	41

1. Introduction

A chemical reaction is a transformation of one substance into another. Such transformations are fundamental for many processes taking place around us. At the molecular level, a reaction involves the breaking and making of chemical bonds, i.e., the way atoms are bonded together in the products is invariably different from their arrangement in the reactants. The aim of research in organic reactivity is to establish what happens at the molecular level in order to understand how the reaction takes place, that is, to find the reaction mechanism. In interpreting experiments, the transition state concept is often used; and its importance derives from the strategic location on the highest point on lowest energy route between reactants and products.

This thesis presents some applications of how quantum chemistry can be used to interpret organic reaction mechanisms. In particular, it is difficult to obtain structural information about the transition state in experiment and, hence, computational modelling can assist and predict organic reactivity.

In chapter 2 the physical background and the approximations needed to arrive at the important concept of a potential energy surface are described. The concept of a global potential energy surface created by the electrons is central to most theoretical descriptions of chemical reactions. Chapter 3 briefly introduces the quantum chemical methods that are used in the computation of reaction mechanisms.

These methods are applied to two radical cation potential energy surfaces in chapter 4. Thus, the quadricyclane radical cation can rearrange to norbornadiene and 1,3,5-cycloheptatriene. Moreover, the ring opening of the bicyclopropylidene radical cation to the tetramethyleneethane radical cation is investigated. A mechanism is favoured by a rehybridization of the olefinic carbons in bicyclopropylidene. Finally, in chapter 5 the principle of least motion is discussed. The material presented in chapters 4 and 5 is based on the articles included in this thesis.

2. Chemical Models

Fact gathering from experiments designed to measure responses of a studied system is one important part of science. But an ingredient of equal importance is the interpretation of these measured facts. The standard procedure is to use a model for ordering an otherwise intractable dataset, and through that added descriptor the measurement can usually be found to follow some underlying principle.

Models are used extensively in science. In general, the primary idea of a model – and what makes it useful – is not the ability to reproduce every detail of the studied object. The value is in its ability to simplify and schematise, that is, to achieve understanding. For a model to be successful and useful it should be easy to remember, simple, self-consistent, powerful and flexible. However, for complex systems it may be necessary to use several different models to capture all the underlying principles of significance.^{1,2}

In such systems the used models are often numerical simulations. This type of computer modelling, or simulation, is normally applied to problems that are too large and complex to perform by hand. In physics and chemistry computational methods, for example, molecular dynamics, Monte Carlo and Car-Parinello,³ are used on a regular basis. In the context of these highly complex computer models it should be stated that models and simulations are best regarded as tools of scientific thinking, and not as giving the true answer to a scientific question. That is, all models or simulations of a natural system are incomplete, since a real system is never closed. A model or simulation that does not contain known or detectable flaws and is internally consistent can therefore be said to be valid, but not verified or true.⁴ Hence, it is only possible to discuss the performance of a model with respect to experimental data, or compare its relative merits to other models for the same system.⁵

Chemistry is not different from the other sciences. It is full of models, of which some well-known examples are the ball and stick model of molecular structure, the periodic table, S_N1/S_N2 reaction mechanisms and molecular orbitals.⁶ Moreover, of particular importance for theoretical and computational descriptions of chemical reactions is the potential energy surface (see later).

Modelling chemical reactions has to deal with the very complex interactions taking place at a reactive event where innumerable molecules interact in gas, liquid or solid phases. Describing how a chemical reaction develops is not straightforward, and can be thought of as a strategic problem, since it often consists of finding a reasonable balance between completeness of describing the interactions involved and the wish to keep the models simple.¹

A. From Quantum Mechanics to Quantum Chemistry

As far as we know, molecules are microscopic particles. Hence, the computational modelling of molecular motions involved in chemistry is ideally based on quantum mechanics, the theory of microscopic physical behaviour. Nonrelativistic quantum mechanics can be completely specified by a couple of known quantities: charge and mass of the electron, the charges and masses of the atomic nuclei and Planck's constant. This theory is most conveniently expressed by the Schrödinger equation

$$i\hbar \frac{\partial \Psi}{\partial t} = H\Psi \quad (1)$$

where

$$H = -\frac{\hbar^2}{2} \sum_{\alpha} M_{\alpha}^{-1} \nabla_{\mathbf{R}_{\alpha}}^2 - \frac{\hbar^2}{2} \sum_j m_e^{-1} \nabla_j^2 - \sum_j \sum_{\alpha} \frac{Z_{\alpha} e^2}{|\mathbf{r}_j - \mathbf{R}_{\alpha}|} + \sum_{j < k} \frac{e^2}{|\mathbf{r}_j - \mathbf{r}_k|} + \sum_{\alpha < \beta} \frac{Z_{\alpha} Z_{\beta} e^2}{|\mathbf{R}_{\alpha} - \mathbf{R}_{\beta}|} \quad (2)$$

The symbols Z_{α} and M_{α} are the atomic number and mass of the α 'th nucleus, \mathbf{R}_{α} is the position of this nucleus, e and m_e are the electron charge and mass, \mathbf{r}_j is the position of the j 'th electron, and \hbar is Planck's constant.

It is often assumed by theoreticians that the Schrödinger equation can explain all chemistry, and it is only the practical problem to solve a complicated differential equation that prevents us from doing so. But there are actually complicated epistemological problems related to the possibility of reducing chemistry into quantum mechanics. That is, reduction of theories is from a philosophical perspective not a trivial problem and already which

type of reduction and what is meant by reduction cause problems and heated arguments.⁷ Nevertheless, the application of quantum mechanics to chemistry does provide much insight.

Thus, to construct a working model for chemical problems several approximations have to be introduced. In the standard procedure the time-dependent part is first separated out, that is, the wave function is factorised, $\Psi(\mathbf{R}, \mathbf{r}; t) = \Psi(\mathbf{R}, \mathbf{r})\Theta(t)$, resulting in two equations

$$\begin{cases} H\Psi(\mathbf{R}, \mathbf{r}) = W\Psi(\mathbf{R}, \mathbf{r}) \\ \Theta(t) = C \exp(-iWt) \end{cases} \quad (3)$$

The time independent equation in (3) is the so-called time-independent Schrödinger equation. The next step is taken by noticing that the lightest nucleus (protium) is at least 1800 times heavier than an electron, and assuming that their motions are usually only weakly coupled, the wave functions of nuclei and electrons can be decoupled. Hence, writing the time-independent wave function as a direct product of separate functions

$$\Psi(\mathbf{R}, \mathbf{r}) = \Psi_{\text{nucl}}(\mathbf{R}) \otimes \Psi_{el}(\mathbf{r}; \mathbf{R}) \quad (4)$$

gives rise to a separation of (3) into an electronic and a nuclear part. This is the Born-Oppenheimer approximation (see later). Note also that there is only a parametric dependence on the nuclear coordinate in $\Psi_{el}(\mathbf{r}; \mathbf{R})$. Moreover, solving the electronic part (the electronic Schrödinger equation) to find the corresponding electronic wave function, $\Psi_{el}(\mathbf{r}; \mathbf{R})$, is called quantum chemistry (see chapter 3).

B. Potential Energy Surface

A potential energy surface (PES) is a concept that simplifies the understanding and interpretation of chemical reactions. The importance of this concept originates from the possibility to link the PES topographic features with the experimentally observed result.

To construct a PES, the nuclear and electronic motions in (3) have to be separated. This type of separation was first used by London in 1929,⁸ by using an adiabatic hypothesis and separating the motion of electrons and nuclei to express how chemical reactions take place in a single electronic

state.* Later on, Eyring and Polanyi⁹ developed this into the first formulation of chemical reaction dynamics, with a multidimensional PES, for the hydrogen-exchange reaction. Since those pioneering studies, it has become the standard model for describing chemical reactions, that is, a chemical reaction is thought of as a motion of the nuclei on a single PES.

Born-Oppenheimer Separation

Potential Energy Surfaces originate from the idea that the proper way to treat molecules in quantum mechanics is to separate the electronic and nuclear motions as far as possible. The first paper dealing with such a separation was Born and Oppenheimer's from 1927,¹⁰ though the approach used nowadays is based on the description given in a book by Born and Huang.¹¹ The physical justification for doing this separation is given by the large difference in electron and nuclear mass. Thus, the electrons move much faster than the nuclei and can therefore adjust rapidly to the much slower nuclear motion.

To decouple the nuclear motion from the electrons, the starting point is (3), and the treatment presented here will be the same as that of Born and Huang. However, their hierarchy of approximations based on perturbation theory and the parameter $(m/M)^{1/4}$ is omitted. For a system of interacting atoms the nonrelativistic Hamiltonian (2) can be rewritten as

$$\begin{aligned}
 H &= -\frac{\hbar^2}{2} \sum_{\alpha} M_{\alpha}^{-1} \nabla_{R_{\alpha}}^2 - \frac{\hbar^2}{2} \sum_j m_e^{-1} \nabla_j^2 + V(\mathbf{r}, \mathbf{R}) \\
 &= -\frac{\hbar^2}{2} \sum_{\alpha} M_{\alpha}^{-1} \nabla_{R_{\alpha}}^2 + H_{el}(\mathbf{r}; \mathbf{R})
 \end{aligned}
 \tag{5}$$

where $V(\mathbf{r}, \mathbf{R})$ includes all interparticle interactions: electron–electron repulsions, electron–nuclear attractions, and nuclear–nuclear repulsions. $H_{el}(\mathbf{r}; \mathbf{R})$ can then be viewed as the Hamiltonian that governs the electrons when the nuclei are fixed at positions \mathbf{R} , i.e., the clamped nucleus approximation. The electronic wave functions $\Phi_j(\mathbf{r}; \mathbf{R})$ are defined as the eigenfunctions of $H_{el}(\mathbf{r}; \mathbf{R})$ for a fixed \mathbf{R}

* The word adiabatic originated in thermodynamics, defined by Clausius in 1850, and refers to thermodynamic changes that have no exchange of heat between the system under consideration and the surroundings. In quantum mechanics, it is associated with gradual changes in a state under a parametric variation of the Hamiltonian of the system.

$$H_{el}(\mathbf{r}; \mathbf{R})\Phi_j(\mathbf{r}; \mathbf{R}) = E_j(\mathbf{R})\Phi_j(\mathbf{r}; \mathbf{R}) \quad (6)$$

where $E_j(\mathbf{R})$ is the PES that corresponds to electronic state j ; and the ground-state ($j = 0$) PES, $E_0(\mathbf{R})$, is the surface of importance for ground state (thermal) reactions. Hence, the $E_j(\mathbf{R})$ for $j \neq 0$, are the PESs corresponding to the excited electronic states, which become important for photochemical reactions. Moreover, the $\Phi_j(\mathbf{r}; \mathbf{R})$ depend only parametrically on the nuclear positions \mathbf{R} , since the nuclear arrangement is clamped and thus, the semicolon in $\Phi_j(\mathbf{r}; \mathbf{R})$.

If the ground and all excited state electronic wave functions $\Phi_j(\mathbf{r}; \mathbf{R})$ are combined, for any fixed \mathbf{R} , they constitute a complete set that spans the Hilbert-space of the electrons; thus the molecular wave function, $\Psi(\mathbf{r}, \mathbf{R})$, is expressed as

$$\Psi(\mathbf{r}, \mathbf{R}) = \sum_i \Phi_i(\mathbf{r}; \mathbf{R})\Omega_i(\mathbf{R}) \quad (7)$$

By substituting (7) into (3), employing the Hamiltonian (5), multiplying from the left by $\Phi_j^*(\mathbf{r}; \mathbf{R})$, and integrating over all electronic coordinates \mathbf{r} , a set of coupled Schrödinger equations for the wave functions $\Omega_j(\mathbf{R})$ is obtained. This describes the nuclear motion on each PES, $E_j(\mathbf{R})$, as

$$\begin{aligned} & -\frac{\hbar^2}{2} \sum_{\alpha} M_{\alpha}^{-1} \nabla_{R_{\alpha}}^2 \Omega_j(\mathbf{R}) + E_j(\mathbf{R})\Omega_j(\mathbf{R}) - W\Omega_j(\mathbf{R}) \\ & = \frac{\hbar^2}{2} \sum_i \mathbf{D}_{ji}(\mathbf{R})\Omega_i(\mathbf{R}) + \hbar^2 \sum_{i \neq j} \mathbf{d}_{ji}(\mathbf{R}) \cdot \nabla_{R_{\alpha}} \Omega_i(\mathbf{R}) \end{aligned} \quad (8)$$

where the first and second derivative matrix elements are defined as

$$\begin{aligned} \mathbf{d}_{ij}(\mathbf{R}) &= -\sum_{\alpha} M_{\alpha}^{-1} \int \{\Phi_i^*(\mathbf{r}; \mathbf{R}) [\nabla_{R_{\alpha}} \Phi_j(\mathbf{r}; \mathbf{R})]\} d\mathbf{r} \\ \mathbf{D}_{ij}(\mathbf{R}) &= -\sum_{\alpha} M_{\alpha}^{-1} \int \{\Phi_i^*(\mathbf{r}; \mathbf{R}) [\nabla_{R_{\alpha}}^2 \Phi_j(\mathbf{r}; \mathbf{R})]\} d\mathbf{r} \end{aligned} \quad (9)$$

Notice that the electronic states $\Phi_i(\mathbf{r}; \mathbf{R})$ and $\Phi_j(\mathbf{r}; \mathbf{R})$ are coupled, as $\Phi_i(\mathbf{r}; \mathbf{R})$ and $\Phi_j(\mathbf{r}; \mathbf{R})$ depend on \mathbf{R} , and this coupling varies as \mathbf{R} changes. Thus, the $\Psi(\mathbf{r}, \mathbf{R})$ function cannot be expressed as a single product $\Omega_i(\mathbf{R})\Phi_i(\mathbf{r}; \mathbf{R})$, and it

requires inclusion of all electronic wave functions to describe a single total molecular wave function. But for the PES-concept to be useful a total wavefunction should be described as a single product, $\Omega_i(\mathbf{R})\Phi_i(\mathbf{r};\mathbf{R})$. To achieve this simplification an approximation is necessary.

If all terms on the right-hand side of the coupled Schrödinger equation (8) are neglected, the Born–Oppenheimer (BO) approximation, this is the equivalent to neglecting all coupling between different electronic and nuclear states. That is, $\Psi(\mathbf{r},\mathbf{R})$ is approximated to the preferred single product form, if $\Phi_i(\mathbf{r};\mathbf{R})$ does not vary much with respect to \mathbf{R} (adiabatic condition). Hence, by solving the electronic Schrödinger equation (6) for the required nuclear geometries, the specific PES, $E_j(\mathbf{R})$, can in principle be computed. The nuclear motion is then governed by a Schrödinger equation

$$\left[-\frac{\hbar^2}{2} \sum_{\alpha} M_{\alpha}^{-1} \nabla_{R_{\alpha}}^2 + E_j(\mathbf{R}) - W \right] \Omega_j(\mathbf{R}) = 0 \quad (10)$$

with a potential given by $E_j(\mathbf{R})$, that is, (10) describes the nuclear motions, i.e., translations,[†] rotations and vibrations, on the potential created by the electrons.

C. Concepts for Chemical Reactions

From the PES a landscape interpretation of chemical reactions appears. This topographical way of approaching reactions is often useful, and it has given rise to several conceptual ideas of which the most important is the transition state that greatly simplifies discussions of chemical reactions.

A PES is a global function of molecular geometry, but certain parts of this surface are more important for describing chemical reactions. The most interesting regions occur around minima and saddle points of first order. Hence, normally the first step in a quantum chemical treatment consists of locating these stationary points. A minimum can represent reactants, products or intermediates. In Figure 1, this is exemplified with one reactant and two product minima (**A** and **B**). A saddle point of first order is defined as the transition structure, if it connects to the corresponding reactants and products, as is shown in Figure 1 where the two transition structures are on the route to **A** and **B**. Furthermore, the stationary points are connected by a

[†] In a strict sense the center-of-mass motion (CM) must be separated out to disentangle the bound states from the continuum, which means removal of the CM translational motion from the internal motions ($H = H_{\text{CM}} + H_{\text{int}}$). Otherwise the associated eigenfunctions $\Psi(\mathbf{r},\mathbf{R})$ will have an infinite norm.

path, often defined as the steepest descent path from the saddle point,¹² illustrated by the two lines in Figure 1, which is often called the reaction path (RP).^{‡13} This path corresponds to the minimum energy that is needed to connect one minimum with another. Actually, in recent years several computational methods have appeared that locate the whole RP from one potential energy minimum to another passing through the saddle point in the same computation.¹⁴

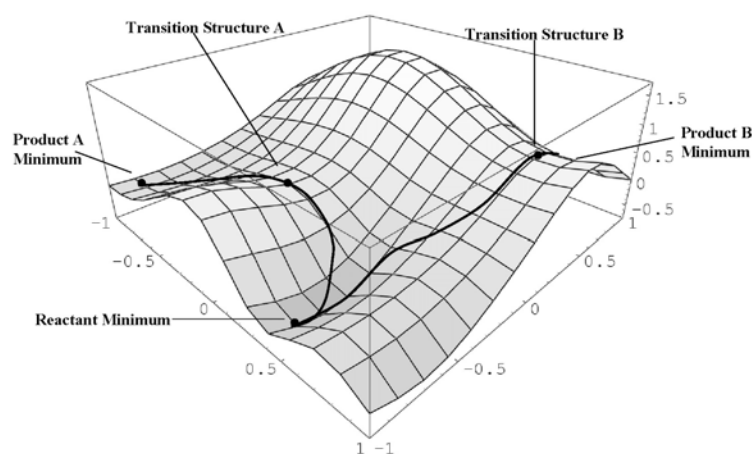


Figure 1. A model PES with minima, transition structures, and reaction paths indicated. If a reactant is transformed into either product **A** or **B**, the chemical reaction is crossing the barrier where the transition structure **A** and **B** are located. The minimal energy path from reactant to the products **A** and **B** are indicated with the two lines on the surface.¹⁵

For empirical studies of chemical reactions a multitude of experimental techniques exists.¹⁶ The main intention with such investigations is to understand how chemical reactions take place, i.e., to find a reaction mechanism. A mechanism is a description of the elementary steps involved in transforming the reactants into products and knowledge of the structure and energies of all species involved. The simplest, and most widely used, way to connect experimental results with the PES molecular model is by transition state theory (TST).¹⁷ Hence, if a chemical reaction is assumed to follow a motion along a path that characterizes the chemical transformation from reactant to product, a transition state is the state at the top of the free energy barrier. In theoretical chemistry an obvious choice is to use the saddle point on the PES as the transition state,¹⁸ although it may often differ from

[‡] The reaction path is also called reaction coordinate or intrinsic reaction coordinate in the literature. The different names are often used synonymously to mean the steepest descent path.

the free energy maximum.¹⁹ An improvement is to transfer the location of the transition state by using any of the variational transition state theories developed to maximize the free energy of activation.²⁰ Yet, in conclusion, the main advantage with TST is the conceptual idea that a specific structure is responsible for the properties of reactivity.

3. Quantum Chemistry

In quantum chemistry (QC) the aim is to find stationary solutions to the Schrödinger equation (1). This section will give a short description of the physical models and approximations that are used to construct approximate quantum mechanical methods for calculating molecular energies and properties.²¹ Since (6) cannot be solved exactly, a general problem in QC is how to include as much as possible of the exact wave function into the models. That is, the approximate solution should ideally retain all symmetries and properties of the exact wave function.²²

In the simplest model the electrons moves in the average field of all other electrons. The mean field model approximates the partial differential equation (6) of $3n$ unknowns, into n functions each depending on three variables. Each such molecular orbital (MO) describes the probability distribution of a single electron. This is the Hartree–Fock (HF) approximation (see later). From this mean field potential and the need to achieve reasonable accuracy, three constructs that characterize QC methods are introduced, i.e., orbitals, configurations, and electron correlation.

Since the interactions between electrons are averaged in HF an error arises. This neglect of the explicit electron–electron interactions due to averaging is usually termed electron correlation energy, which is defined as the difference between the exact nonrelativistic energy and the HF energy. Corrections to HF must therefore include details of such electron correlations. In the most used approaches these effects are incorporated by either an expansion of the HF configuration, e.g., perturbation theory and coupled cluster, or to improve on the HF description as in Kohn–Sham density functional theory. Methods that incorporate electron correlation are important for accurate and quantitative evaluation of molecular energies.

Another approximation is needed to simplify the solution on computers. It is advantageous to expand the MO functions in a given fixed finite set of functions. Such functions are usually called the atomic orbital (AO) basis. Normally, AO functions are Gaussian functions, or linear combination of Gaussians, since this form permits all required matrix elements to be evaluated analytically. The combination of these two approximations, i.e., to solve an approximative set of equations and use an incomplete set of expansion functions for the MOs, is in principle the source for errors in QC.

A. Methods

In QC there are some standard models for the construction of approximate wave functions. At the simplest level the wave function is represented by a single Slater determinant, that is, the HF model. In the more complex post Hartree-Fock models the HF wave function is usually determined by a superposition of several Slater determinants.²³ Finally, in the density functional theory approximate forms of the electron density are used to compute the molecular energies.²⁴

Hartree-Fock

The HF wave function is an antisymmetrised product of one-electron spin functions

$$\Psi_{HF} = |\chi_1 \dots \chi_N\rangle \quad (11)$$

where the spin orbitals χ_j form a Slater determinant. By applying the variational principle

$$E = \frac{\langle \Psi | H | \Psi \rangle}{\langle \Psi | \Psi \rangle} \quad (12)$$

one can derive equations, termed the Hartree-Fock (HF) equations, which determine the optimal spin orbitals by minimising the value of E with respect to the choice of spin orbitals.²³ The HF method is a mean field method applied to the many-electron problem and is therefore often called the self-consistent field (SCF) method.

The accuracy of a calculation with approximate methods should not degrade as the molecular system becomes larger. That is, the energy should scale extensively with the number of electrons ("size extensivity"), or essentially equivalently, the energy of a system of noninteracting fragments should be exactly the sum of separate calculations on the fragments ("size consistency"). In HF the size scaling is satisfied, but for several of the correlation methods this is not the case.²⁵

Post Hartree-Fock

The post HF methods (MP2 and CCSD(T)) used in this thesis are size extensive. The simplest way to introduce the correlation energy unaccounted for in HF, is by the Møller-Plesset perturbation theory (MP).

MP consists in applying the Rayleigh–Schrödinger perturbation theory using the Fock operator as the zeroth-order Hamiltonian and a Slater determinant of spin orbitals as the zeroth-order wave function. The total electronic energy is given by the sum

$$E = E^{(0)} + E^{(1)} + E^{(2)} + E^{(3)} + E^{(4)} + \dots \quad (13)$$

The zeroth-order energy is the sum of the eigenvalues of the occupied spin orbitals, and the sum of the zeroth- and first-order energies is the HF energy. The sum of the remaining terms in the series is the correlation energy that MP theory is able to recover.

The simplest MP treatment is second-order (MP2). Since the HF wave function has no matrix elements with single excitations, the leading corrections due to electron correlation are doubly substituted determinants that correspond to electron pair excitations. In MP2 theory a simple and tractable expression for the correlation energy is given, which is moderately successful for cases where the HF determinant is a qualitatively correct starting point. It recovers ~80 % of the correlation energy per electron pair.

It should be noted that the MP formalism is potentially rather dangerous in design. All perturbation theories work best when the perturbation is small. But in the case of MP theory, the perturbation is the full electron–electron repulsion energy, which can be a large contributor to the total energy. So, there is no reason to expect that an MP2 calculation will give a value for the correlation energy that is very good. In addition, MP_n methodology is *not* variational. Thus, it is possible that the MP2 estimate for the correlation energy will be too large instead of too small. However, this is rarely the case in practice, because basis set limitations always introduce an error that is underestimating the correlation energy.

The other post-HF method used to recover correlation energy in this thesis is the coupled-cluster (CC) theory. Since the most effective way to construct a wave function that is size extensive is to consider a trial function where the expansion (excitation) operators are exponentiated. The CC theory is defined as

$$\Psi = e^{\mathbf{T}} \Psi_{\text{HF}} \quad (14)$$

and the cluster operator is

$$\mathbf{T} = \mathbf{T}_1 + \mathbf{T}_2 + \mathbf{T}_3 + \dots + \mathbf{T}_N \quad (15)$$

where N is the total number of electrons and the various \mathbf{T}_i operators generate all possible determinants having i excitations from the reference. The possibility to truncate \mathbf{T} in a size extensive manner is the great advantage with CC theory. Considering a trial wave function in which the single and double excitation operators are exponentiated, one defines the coupled-cluster method limited to single and double replacements (CCSD).

$$\Psi_{\text{CCSD}} = e^{\mathbf{T}_1 + \mathbf{T}_2} \Psi_{\text{HF}} \quad (16)$$

CCSD is size extensive, but the single and double substitution coefficients contained in the \mathbf{T}_1 and \mathbf{T}_2 operators are not variationally determined. Moreover, in various approaches, estimates of the connected triples using perturbation theory have been proposed. The most robust one is the so-called CCSD(T) method,²⁶ and indeed, for high accuracy the CCSD(T) level has become the most used single-reference method.

For molecules at their equilibrium geometry, CCSD recovers ~95 % of the ground state correlation energy in a given basis. A further improvement is possible when CCSD is corrected with perturbative estimates of the triples in CCSD(T). This level gives an accurate treatment of electron correlation for molecules near their equilibrium geometries provided sufficiently large basis sets are employed.

Density Functional Theory

In density functional theory (DFT) the electronic energy is a functional of the electron density instead of the wave function. The electron density is only a function of three variables, compared to the $3n$ variables involved in the n -electron wavefunction. So DFT has the potential to dramatically simplify QC calculations.

The electron density $\rho(\mathbf{r})$ is a variable in the real three-dimensional space. Present day DFT is based on two fundamental theorems. First, the Hohenberg–Kohn theorem, which states that the exact ground state energy of a molecular system is a functional only of the electron density and the fixed positions of the nuclei. In other words, for some fixed nuclear coordinates, the electron density uniquely determines the energy and all properties of the ground state. Second, the exact electron density function is the one that minimises the energy (i.e., as a functional of the density), thereby providing a variational principle to find the density.

The challenge in DFT is to design accurate functionals. In Kohn–Sham (KS) DFT an artificial reference system of noninteracting electrons is constructed, which has exactly the same electron density as the real molecular system of interacting electrons. The kinetic energy is

approximated as that of the noninteracting reference system, which can be evaluated in terms of the KS orbitals.

The total energy from the Schrödinger equation can be decomposed into

$$E[\rho] = T[\rho] + V_{\text{en}}[\rho] + J[\rho] + E_{\text{XC}}[\rho] \quad (17)$$

where T is the kinetic energy, V_{en} is the electron–nuclear interaction, J is the Coulomb repulsion plus nonclassical terms due to correlation and E_{XC} exchange effects included in the exchange–correlation (XC) energy. To make a concrete use of DFT an effective approximation to E_{XC} in the KS formulation is needed.

If the exchange–correlation energy of an inhomogeneous system, such as an atom or a molecule, is estimated by the integral

$$E_{\text{XC}}^{\text{LDA}} = \int \varepsilon_{\text{XC}}[\rho^\alpha(\mathbf{r}), \rho^\beta(\mathbf{r})] \rho(\mathbf{r}) d^3\mathbf{r} \quad (18)$$

where the integrand samples the local spin-densities $\rho^\alpha(\mathbf{r})$ and $\rho^\beta(\mathbf{r})$ at each integration point \mathbf{r} , we have the local spin-density approximation (LSDA) of DFT.²⁷ Another estimate of the exchange–correlation energy for an inhomogeneous system is

$$E_{\text{XC}}^{\text{GGA}} = \int f_{\text{XC}}(\rho^\alpha(\mathbf{r}), \rho^\beta(\mathbf{r}), |\rho^\alpha(\mathbf{r})|, |\rho^\beta(\mathbf{r})|) d^3\mathbf{r} \quad (19)$$

where the integrand f_{XC} depends on the spin densities and their gradients, called the generalized gradient approximation (GGA).²⁷ Becke introduced some numerical fitting parameters in GGA's that he determined by optimising the accuracy of atomisation energies of a standard set of molecules. He also introduced a hybrid method, i.e., the B3LYP functional, where the exchange–correlation expression contains a parameter a_0 to include nonlocality in the exchange–correlation hole

$$E_{\text{XC}}^{\text{Hyb}} = E_{\text{XC}}^{\text{DFT}} + a_0(E_{\text{X}}^{\text{Exact}} - E_{\text{X}}^{\text{DFT}}) \quad (20)$$

Such hybrid approximations reduce the average bond energy error from about 6 kcal/mol for pure GGA's to roughly 2 kcal/mol. Reaction barrier heights are also improved by exchange mixing. With DFT it is possible to solve many electron problems in QC at an accuracy comparable to the MP2 method. But because the explicit construction of the wave function is avoided, the basis set requirements for DFT are more modest than what is needed to obtain reliable results with MP2.

B. Basis sets

QC calculations usually employ expansions of AOs in basis sets. The most used ones are either of Slater type or of Cartesian Gaussian type.²⁸

The Slater-type orbitals (STO) constitute a very good AO basis for atomic and molecular calculations. This is because an STO, which is an exponential function, fulfils the requirement of a correct asymptotic behaviour both at the atomic nucleus and at large distances. However, handling molecular integrals over STO is very inefficient.

The Gaussian-type AOs (GTO) reduce the complexity of the mathematical integration problem. A GTO does neither exhibit a correct asymptotic behaviour at large distances, nor does it satisfy the cusp condition at the origin. Therefore, several GTOs have to be used in order to describe the AOs correctly. To construct GTO basis sets the most common approach is to use linear combinations (contractions) of individual GTO (primitives). By this way, the standard basis sets are built up and are available as basis set libraries in computer programs for QC calculations.

For instance, in the 6-31G basis set, a contraction of six GTO is used to describe the core AOs to compensate for the missing cusp at the origin. The valence AOs are described by two sets of GTO: a contraction of three primitives, and an uncontracted Gaussian function. Hence, 6-31G is a so-called split valence or double zeta (DZ) valence basis set. Since two AOs with different orbital exponents ζ are used to simulate the valence AOs. On the next level of basis set, the 6-311G is a triple zeta (TZ) valence basis set and is therefore more flexible than 6-31G.

The flexibility of split valence basis sets is enhanced by the use of polarization functions. Such functions allow more flexibility to better account for the distortion of the MOs in molecules. In 6-31G(d,p), for instance, a set of d-type orbitals is added on first-row atoms, and a set of p-type orbitals is added on the hydrogen atoms. That is, 6-31G(d,p) is a basis set of valence double zeta plus polarization (VDZP) quality. The basis set can be augmented further, in particular to describe anions and Rydberg excited states correctly, with orbitals which have small exponents, resulting in large diffuse functions. In 6-311+G(d,p), a diffuse function is added on each heavy atom in the molecule. Moreover, in Dunning's correlation consistent (cc) basis sets, all basis functions which make correlation energy contributions of similar size are added together. The cc-pVDZ basis set, for example, is of split-valence (DZ) plus polarization type, and is formed by adding a set of (spd) primitives to the atomic HF orbitals. The exponents for the correlation functions are optimized from correlated calculations on the atoms.

C. Spin Density and Hyperfine Coupling Constants

The spin density is defined as the excess α spin density over that of the β spin at a given point of a radical

$$\rho(\mathbf{r}_N) = \rho^\alpha(\mathbf{r}_N) - \rho^\beta(\mathbf{r}_N) \quad (21)$$

An isotropic hyperfine coupling constant (hfcc) measures a net unpaired electron density at a particular nucleus.²⁹

In QC calculations the hfcc of a certain nucleus N is given by the Fermi contact interaction³⁰

$$a_N(iso) = \frac{8\pi}{3} g_e \mu_B g_N \mu_n \rho(\mathbf{r}_N) \quad (22)$$

where the hfcc $a_N(iso)$ is in Gauss. In (22) g_e is the g value of the electron in the radical, g_N is the g value of nucleus N , and μ_B and μ_n are the Bohr and the nuclear magnetons, respectively. The theoretical determination of the hfccs is a difficult task. Reliable hfccs require the inclusion of both correlation corrections and inner-shell spin polarization effects combined with a certain flexibility of the basis set employed.³¹ Yet, very good results are obtained with the B3LYP functional in the calculation of hfccs.³²

4. Radical Cation Rearrangements

Radical cations are important intermediates in many chemical and biological processes. For instance, in photosynthesis, redox enzymes, and electron transfer chemistry. The unpaired electron in these species often makes them very reactive, which can be a nuisance because it makes the reactive events hard to control, but it can also be advantageous since it gives rise to very effective transformations.³³ Moreover, radical cations are often unstable species that undergo rapid rearrangements. Such rapid structural reorganization makes experimental studies difficult and is a limiting factor in the understanding of electronic structure and stability.

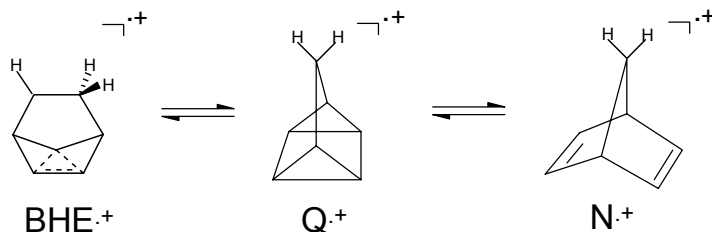
The rapid rearrangement indicates that the activation energy is considerably lower than for the neutral equivalent. In several systems this lowered activation energy occurs for an unexpected reaction path, which can give rise to structures without neutral precedents.³⁴ Another particular feature of organic radical cations is that novel types of mechanisms are not uncommon. Both systems discussed in this chapter serve as good illustrations of these very particular characteristics of radical cations. Computational studies have been performed on the quadricyclane radical cation (Q^+) (Paper I, II and III) and the bicyclopropylidene radical cation (BCP^+) (Paper IV) rearrangements.

A. Quadricyclane Rearrangements to 1,3,5-Cycloheptatriene and Norbornadiene

The Q^+ conversion to the norbornadiene radical cation (N^+) is a prototype of one-electron oxidation reactions. Actually, it was not until 1994 that a direct observation of Q^+ was reported using electron spin resonance (ESR) spectroscopy, and the signal disappears after $\sim 1.5\mu s$ at room temperature.^{35,36} The computational studies performed on this cycloreversion agree with the experimental observation that Q^+ is an unstable species, with an estimated activation energy in the range 5-12 kcal/mol, and the cycloreversion takes place through a concerted mechanism with a pseudo-Jahn–Teller distorted transition structure.³⁷

However, in several studies, additional radical cation species have been observed when starting from Q^+ .^{36,38,39,40,41} From ESR studies in a CF_3CCl_3 matrix it was proposed that these additional species were the bicyclo[3.2.0]hepta-2,6-diene (BHD^+) and the 1,3,5-cycloheptatriene (CHT^+) radical cations.³⁸ The 1H hyperfine coupling constants (hfcc) were later confirmed by ESR measurements in zeolites, and the conversion was measured to always be less than 3% of concentration.^{36,39} Interestingly, if Q is isopropylidene-substituted, the one-electron oxidation reaction gives only BHD as product, in quantitative yield.⁴²

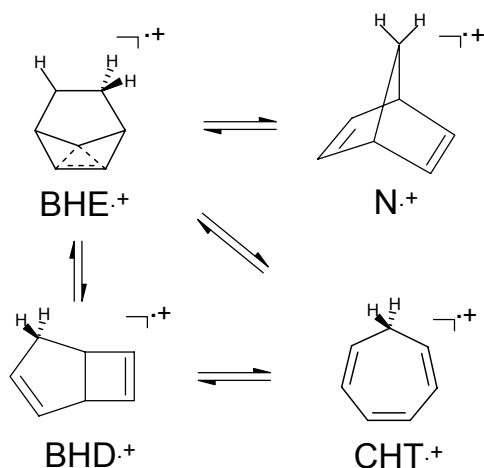
In the computational studies of the $C_7H_8^+$ PES (Paper I, II and III) we have established plausible mechanisms for some alternative rearrangements. Thus, in Q^+ one of the four lateral bonds in the cyclopropane units is broken and the bicyclo[2.2.1]hepta-2-ene-5-yl-7-yl-ium radical cation (BHE^+) is formed. The free energy barrier for this bond breaking is 14.9 kcal/mol. Moreover, we found that BHE^+ is more stable than BHD^+ , and by comparing with the hfcc previously assigned to BHD^+ we find that they agree much better with BHE^+ . It is therefore concluded that the two rearrangement paths from Q^+ lead either to the major product N^+ or to BHE^+ .



From BHE^+ two reaction paths lead to CHT^+ , i.e., one multistep rearrangement with two shallow minima, and one stepwise rearrangement through BHD^+ with the electrocyclic ring opening. The multistep path has a rate-limiting step with 16.5 kcal/mol activation energy, which is 2.8 kcal/mol lower than for the stepwise mechanism. Furthermore, we also located a concerted transformation of BHE^+ into N^+ that has 20.0 kcal/mol activation energy.

This other $C_7H_8^+$ Q^+/CHT^+ rearrangement chemistry has attracted less attention than the Q^+/N^+ , but it could give valuable information of the different side products that can be expected upon substitution and environmental changes. One example that underscores this is that isopropylidene substituted Q rearranges to BHD as the major product, instead of the expected N , for one-electron oxidation reactions.⁴² Another example is that CHT^+ is observed together with BHE^+ and several

deprotonated neutral radicals in ESR studies of \mathbf{Q}^+ and \mathbf{N}^+ in different matrices.^{38,39} Moreover, ESR studies of \mathbf{BHD} in a CFCl_3 matrix give, after γ -irradiation, the hfcc assigned to \mathbf{BHE}^+ together with a hfcc assigned to \mathbf{CHT}^+ .⁴³ This observation of \mathbf{CHT}^+ was ascribed to an electrocyclic ring opening of \mathbf{BHD}^+ , but in our calculations the transformation is most likely to occur through the multistep path.



An energy profile for the activation energies at 100 K for the cycloreversion (\mathbf{Q}^+ , $\mathbf{TS1}$, \mathbf{N}^+) and the skeletal rearrangement (\mathbf{Q}^+ , $\mathbf{TS2}$, \mathbf{BHE}^+) is shown in Figure 2. This free energy profile contains the zero-point correction, and the free energy thermal correction calculated from the B3LYP/6-311G(d,p) frequencies, and the electronic energies taken from CCSD(T)/6-311G(d,p)//B3LYP/6-311G(d,p) calculations.

The geometries for the cycloreversion path are in good agreement with the previous results.³⁷ That is, $\mathbf{TS1}$ shows a pseudo Jahn-Teller distorted transition structure with elongated bonds in the four-membered ring. The activation energy becomes 10.1 kcal/mol, which agree well with the earlier estimated computational activation energies in the range 5-12 kcal/mol and the experimental estimate of 9.3 kcal/mol.⁴²

The skeletal rearrangement to \mathbf{BHE}^+ has a transition state, $\mathbf{TS2}$, where one of the four lateral bonds in the cyclopropane units in \mathbf{Q}^+ has opened to a distance of 2.13 Å. Breaking this bond costs more energy than for the pericyclic cycloreversion, since the estimated free energy of activation is 14.9 kcal/mol. Hence, the skeletal rearrangement has 4.8 kcal/mol higher activation energy than the cycloreversion (see Figure 2).

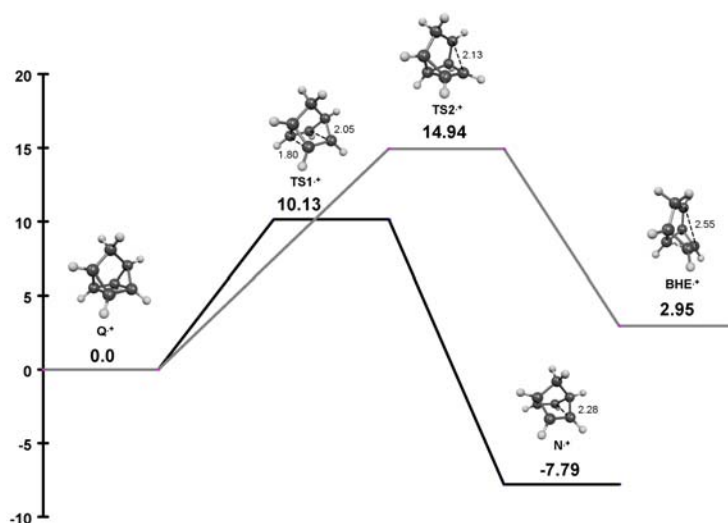


Figure 2. Free energy profiles for the two \mathbf{Q}^+ isomerizations, a cycloreversion (**TS1**) to \mathbf{N}^+ and a skeletal rearrangement (**TS2**) to \mathbf{BHE}^+ (kcal/mol).

Among the rearrangements that continue from \mathbf{BHE}^+ (see Figure 3) the multistep path is the most favourable with an activation energy of 16.5 kcal/mol above \mathbf{Q}^+ for its rate-limiting step, **TS7**. It has 2.8 kcal/mol lower activation energy than the stepwise, and 3.4 kcal/mol lower than the concerted path to \mathbf{N}^+ , as can be noticed in Figure 3. The other two routes that branch out from \mathbf{BHE}^+ are: the stepwise mechanism (\mathbf{BHE}^+ , **TS3**, \mathbf{BHD}^+ , **TS5**, \mathbf{CHT}^+); and the concerted path (\mathbf{BHE}^+ , **TS4**, \mathbf{N}^+). Both break the three-center two-electron bond by following different internal coordinates than the multistep path (see later). The stepwise mechanism has a low barrier of 10.2 kcal/mol to form \mathbf{BHD}^+ and an electrocyclic ring opening, **TS5**, which is rate-limiting. This first step is before **TS3**, a formation of a cyclopropane unit, and after **TS3** a breaking of one bond in this cyclopropane (see Figure 3). For the concerted path the three-center two-electron bond breaks before the transition state, **TS4**, and one bond forms and another breaks to form \mathbf{N}^+ after **TS4**.

Multistep Rearrangement

The multistep rearrangement transforms \mathbf{BHE}^+ into \mathbf{CHT}^+ through two routes: (\mathbf{BHE}^+ , **TS6**, **I1**, **TS7**, **I2**, **TS9**, \mathbf{CHT}^+) and (\mathbf{BHE}^+ , **TS6**, **I1**, **TS8**, \mathbf{CHT}^+). The B3LYP/6-311+G(d,p) stationary points involved in the rearrangement are shown in Figure 4 and 5. In the first step, an almost complete bond breakage of the C4-C7 bond from 1.54 Å in \mathbf{BHE}^+ to 1.93 Å for the C2-C7 distance in **TS6**. At the same time, the three-center two-

electron bond distances (C2-C7 = 1.74 Å, C3-C7 = 1.73 Å) change into distances in **TS6** (C1-C7 = 1.58 Å, C6-C7 = 1.52 Å) more reflecting ordinary C-C single bonds. In the first intermediate, **I1**, this process has continued, and this distance (C2-C7 for **I1**) is 2.44 Å but also the C1-C7 bond has become elongated to 1.63 Å. This intermediate is in a very shallow minimum, with **TS6** being structurally similar to **I1**, there is only a 1.3 kcal/mol free energy barrier for the reversion to **BHE**⁺. The small imaginary frequency of -391.2 cm^{-1} for **TS6** and the lowest frequency for **I1** of 217.4 cm^{-1} both reflect the shallow well on the reaction path since these normal modes closely mimic the reaction path.

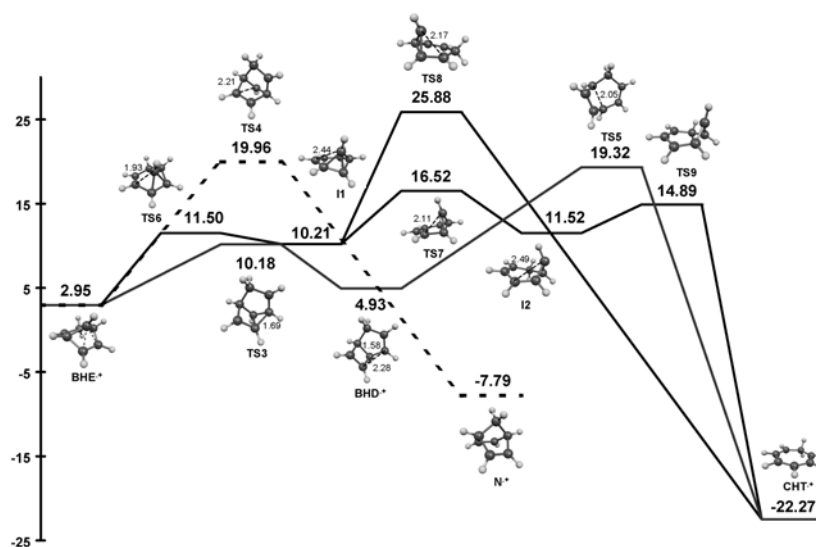


Figure 3. Comparison of the multistep (**BHE**⁺, **TS6**, **I1**, **TS7**, **I2**, **TS9**, **CHT**⁺) and (**BHE**⁺, **TS6**, **I1**, **TS8**, **CHT**⁺), stepwise (**BHE**⁺, **TS3**, **BHD**⁺, **TS5**, **CHT**⁺) and concerted (**BHE**⁺, **TS4**, **N**⁺) rearrangement free energy profiles in kcal/mol.

From **I1** this isomerization path splits into two routes with transition states **TS7** and **TS8**, which both have similar mechanisms, but break bonds on opposite sides. In **TS7**, the C1-C7 bond of **I1** is opened to 2.11 Å, and in **TS8** the C5-C7 bond of **I1** is opened to 2.17 Å. Although the major coordinates involved in the respective mechanism show strong similarities, the difference in reaction barrier of 9.36 kcal/mol (see Figure 3) implies that the differences in mechanism give rise to a large energy difference. For instance, the **I1** C1-C7 bond is elongated compared to a normal C-C single bond distance in the C5-C7 bond, and between **I1** and **TS8** the six-membered ring has to invert as is reflected in $\phi(4,5,1,2) = -16.0^\circ$ for **I1** and $\phi(4,5,1,2) = 16.9^\circ$ for **TS8**. Both **TS7** and **TS8** have small imaginary

frequencies, -309.9 cm^{-1} and -259.5 cm^{-1} , with normal modes that closely follow the reaction coordinates.

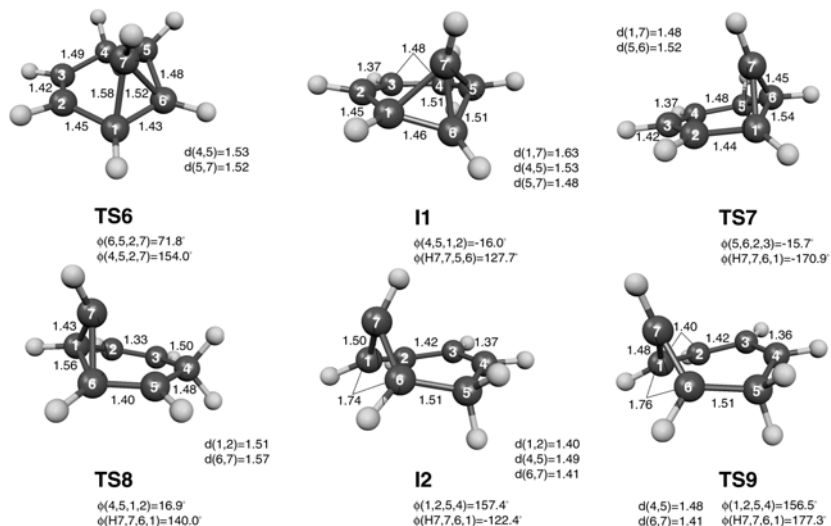


Figure 4. B3LYP/6-311+G(d,p) optimized stationary points for the multistep rearrangement.

The **TS8** route leads directly to **CHT⁺**, while the **TS7** route isomerizes to another shallow intermediate, **I2**. The distance for the bond broken from **I1** to **TS7** becomes even longer, 2.49 \AA , because of the rearranging carbon skeleton and a partly broken C1-C6 bond. Thus, in **I2** the six-membered ring is slightly folded, $\phi(1,2,5,4) = 157.4^\circ$, and the C1-C6 bond is opened to 1.74 \AA . Moreover, **I2** has several low vibrational frequencies (180.8 , 223.8 , 319.9 and 378.2 cm^{-1}) and their corresponding normal modes indicate that the floppy directions include both carbon skeletal motions and H7 motions.

The last step in this rearrangement is the complete opening of the C1-C6 bond and flattening of the carbon framework into the **CHT⁺** C_{2v} geometry. In this mechanistic step **TS9** is a very early transition state. The dominating change on the reaction path up to **TS9** is a hybridization change of C7 from being pyramidalized in **I2** to sp^2 in **TS9**. This is, furthermore, reflected in the normal mode with imaginary frequency, -607.7 cm^{-1} , that has a dominating contribution for this pyramidalization movement, and a very minor component of opening and flattening of the carbon skeleton.

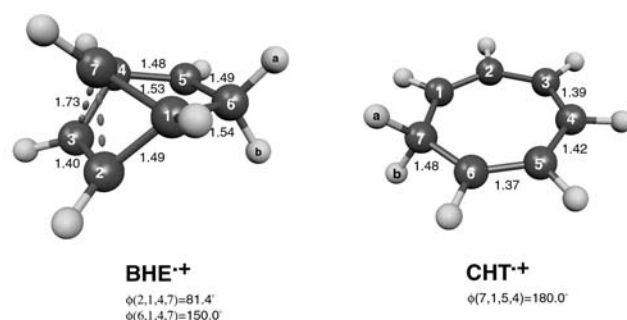


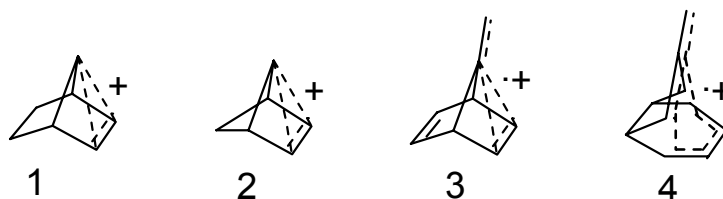
Figure 5. B3LYP/6-311+G(d,p) optimized stable structures of **BHE**⁺ and **CHT**⁺.

Bicyclo[2.2.1]hepta-2-ene-5-yl-7-ylum radical cation

The geometry of **BHE**⁺ shows special characteristics (Figure 5). By using natural bond orbital (NBO) analysis we outlined the bonding and electronic structure of this radical cation.

Its geometry has similarities with **N**⁺, but presents two striking differences. The most obvious one is the strong tilting of the C7 bridge towards the C2-C3 bond, which is shown by the difference between the two dihedral angles, ϕ_1 and ϕ_2 . This tilting also affects the C2-C3 bond, which has a length of 1.40 Å, indicating an elongated double bond. The other difference between **BHE**⁺ and **N**⁺ is the C5 and C6 coordination: C5 is a three-coordinated carbon with bonds that are only partly shortened C-C single-bonds, and it does not show any pyramidalization; C6 is similar to the methyl carbons found in norbornenyl.

In carbocation chemistry this type of structure is well known from both experiment and computations.⁴⁴ Two examples that show a behaviour similar to **BHE**⁺ are the 7-norbornenyl cation, **1**, and the bicyclo[2.1.1]hex-2-en-5-ylum cation, **2**. These two examples are verified with both experiment and calculations to have structures and properties that show the characteristics of a so-called bishomoaromatic three-center two-electron bond. **BHE**⁺ shows a strong resemblance in its geometric parameters with the bonds formed in the two cations **1** and **2**, and we therefore assume that **BHE**⁺ should have a similar bishomoaromatic, three-center two-electron bond between C2-C3-C7 with a strong cationic behaviour.



A homoaromatic interaction is a kind of conjugative stabilization where the p-orbital overlap shows a discontinuity from the presence of a sp^3 hybridized atom. That is, the p-orbital overlap bridges the sp^3 centre and aromatic features are manifested. In theoretical terms this is an increased stabilization through a delocalisation of electron density, and it should also cause a distortion of the geometry.

Actually, this type of conjugative stabilization has also been suggested for radical cations.⁴⁵ Of particular interest for this work is the exocyclic stabilization, between C2-C3 and the C7-C8 double bonds, in 7-methylenenorbornene, and 7-methylenenorbornadiene, **3**. Another example of a bishomoaromatic stabilization is the bishomoheptafulvene, **4**. However, none of these examples are as well documented as the bishomoaromatic carbocation structures.

In the NBO analysis the purpose is to find the NBO Lewis structure (LS), i.e., to construct localized chemical bonds and lone pairs from the delocalized molecular orbitals. For open-shell systems this is done with the different hybrids for different spins NBO, which yields separate LSs for α and β spin. In **BHE**⁺ both α and β LSs have similar NBOs if the three-center search is added, with only relatively small polarizations, and no bonds with low occupancy appear. Moreover, most of the located bonds are of σ_{C-C} or σ_{C-H} type, with two important exceptions (see below). The two σ -bonds with the lowest electron occupation are the σ_{C1-C7} ($\alpha = 0.952e$, $\beta = 0.953e$) and σ_{C4-C7} ($\alpha = 0.951e$, $\beta = 0.942e$), which in both cases is close to a two electron Lewis bond. Therefore the NBO located σ -bonds indicate a σ -bonded backbone that has little radical character.

The special characteristics of **BHE**⁺ can be explained by the two remaining occupied NBOs. First, a three-center NBO between C2-C3-C7, plotted to the left in Figure 6 (with electron occupation: $\alpha = 0.974e$, and $\beta = 0.976e$), is responsible for the C7 tilt towards C2-C3. Further, a 0.64 positive charge is located around the C2-C3-C7-bond[§] using natural population analysis, implying a large cationic character in this part of the molecule. Second, a nonbonding orbital, n_5 , is located on C5, plotted on the right in Figure 6 (with electron occupation $\alpha = 0.918e$ and $\beta = 0.074e$). Hence, most of the radical character is localized on n_5 , with less positive charge localized (0.18) on this part.

In conclusion, the spin and charge are to a large extent separated in **BHE**⁺. That is, this is a bishomoaromatic distonic radical cation, with the

[§] This value was obtained by summing up the natural population charges for α and β spin for C2(-0.01, -0.02), C3(-0.05, 0.02), C7(-0.03, 0.00), H2(0.13, 0.13), H3(0.13, 0.14), and H7(0.14, 0.14). Another area where a substantial part of the positive charge is located is around C5-H5 (0.18): C5(-0.50, 0.42), H5(0.11, 0.14); the remaining charge (0.18) is delocalized.

radical character localized in the singly occupied orbital, n_5 , and the charge localized in the three-center bond.

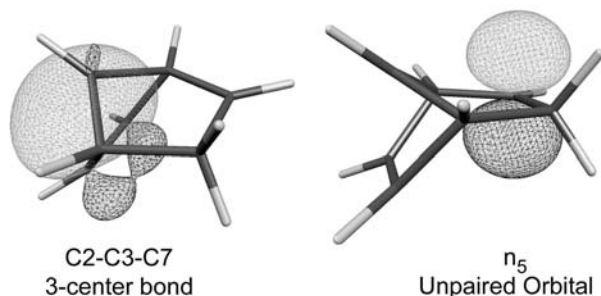


Figure 6. Contour plots of the α -PNBO for the three-center bond, and the singly occupied orbital. The PNBOs are taken from a B3LYP/6-311+G(d,p) NBO-calculation.

B. Bicyclopropylidene: a Rehybridization Ring Opening to Tetramethyleneethane

The chemistry of cyclopropane rings has attracted significant interest, both as being theoretically interesting and for more practical purposes.⁴⁶ In cyclopropane radical cation chemistry, systems that contain olefinic moieties present a particularly challenging class and their reactivity involves several interesting features.³⁴ Bicyclopropylidene (**BCP**) is one such example, which has two cyclopropylidene rings connected by a shared C–C double bond. In matrix isolation experiments the **BCP**⁺ ring opening to the tetramethyleneethane radical cation (**TME**⁺) is observed after γ -irradiation of **BCP**.⁴⁷

The **BCP**⁺ structure relaxes from the planar **BCP** to a twisted conformation, as is expected in alkene radical cations.⁴⁸ But in alkenes the C–C double bond is also substantially elongated compared to the neutral geometry, which is not observed for **BCP**⁺ where the elongation is only 0.06 Å (with B3LYP/6-31G(d,p)). Moreover, the proximal bonds (C1–C2, C1–C3, C1'–C2', C1'–C3') are elongated, and the distal bonds (C2–C3, C2'–C3') are shortened (see Figure 7 for the optimized **BCP** structures).

NBO analysis interprets both the small elongation of C1–C1' and distal bond elongation as due to hyperconjugation. Thus, if the total NBO occupation between C1–C1' are summed, the population becomes 3.490e, which is only $\sim 0.5e$ less than for a neutral C–C double bond. That is, $\sim 0.5e$ are transferred from the cyclopropane rings into the different C1–C1' bonds, and, hence, result in a large depletion of electron density in the σ -bonded

backbone. In particular, the longer proximal bonds can be interpreted by a large hyperconjugative effect between the β -spin in these bonds into n_1 and n_1' (which are nonbonding NBOs located on C1 and C1'). This gives rise to a depleted β -population, and therefore longer proximal bonds.

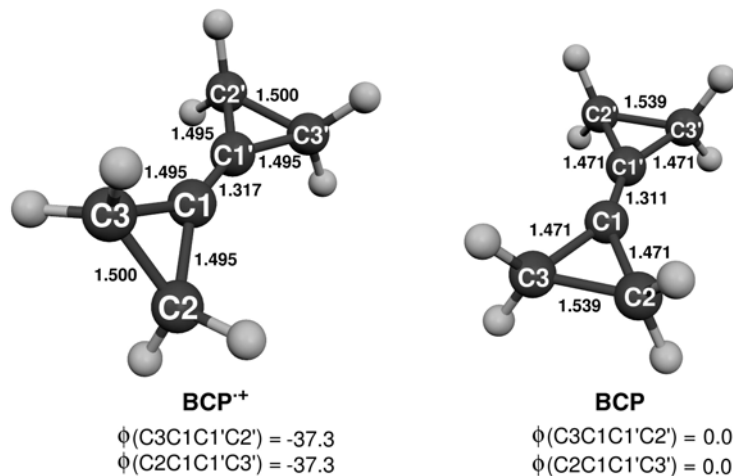


Figure 7. B3LYP/6-31G(d,p) optimized minima of **BCP⁺** and **BCP**.

The two ring openings from **BCP⁺** to **TME⁺** follow a stepwise mechanism with a rehybridization of the olefinic carbons, C1 and C1'. In Figure 8, the free energy profile of this ring opening is displayed, and the relevant geometries are indicated (**1-10**).

During the opening of the first ring (**1**, **5**, **6**, **7** and **8**) the activation energy is 7.3 kcal/mol. There are several coordinates involved in this stepwise process. In the first step, the reaction path alters its character around **5**: before **5**, the major reaction coordinate is a rehybridization of the sp^2 -C1 in **1** to a pyramidalized C1 in **5**. After this transition state the C2-C3 bond elongation is the dominating change to the very shallow minimum **6**. Actually, the free energy of **6** is only 0.5 kcal/mol lower than **5** and is slightly higher (~ 0.1 kcal/mol) than **7**. The second step proceeds without barrier, and the main coordinates are a continued elongation together with a flattening back to sp^2 -hybridization of C1. At the local minimum **8**, ~ 14 kcal/mol below the **5-6-7** plateau, the C2-C3 bond is completely broken, and the carbon skeleton forms a plane that also contains the H-atoms on C2 and C3. That is, **8** has acquired a **TME⁺** character around C1C2C3 while keeping a **BCP⁺** character around C1'C2'C3'.

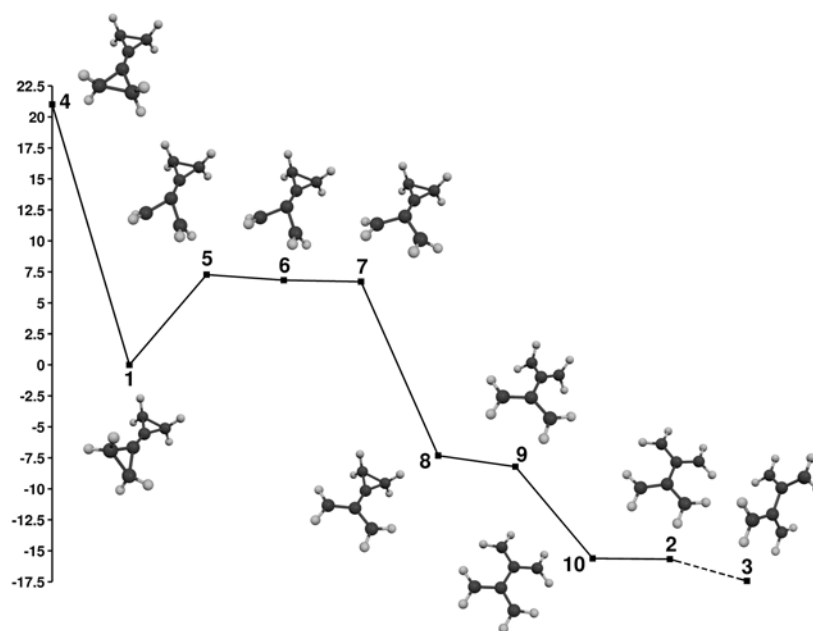


Figure 8. Free energy profile of the stepwise BCP^+ to TME^+ reaction path, in kcal/mol relative to BCP^+ (**1**). The other geometries are: ionised BCP (**4**), TME^+ (**2**, **3**), transition states (**5**, **7**, **9**, **10**) and minima (**6**, **8**).

As can be seen in Figure 8 the second ring opening to TME^+ (**8**, **9**, **10**, **2**) is barrierless. Yet, the mechanism is a similar rehybridization as in the first ring opening. The transition state, **9**, characterized as such by both B3LYP and MP2, has a 1.1 kcal/mol barrier (B3LYP), no barrier (MP2), and is 1.1 kcal/mol lower than **8** (CCSD(T)) for the reaction path from **8** to **2**, which indicates that **8** is not a stable intermediate. After **9**, a bifurcation transition state, **10**, is found. This stationary point has a low imaginary frequency (-33 cm^{-1}), corresponding to rotation around C1-C1' , which reflects that a TME^+ minimum, **2**, is reached by a $\sim 10^\circ$ torsion and with ~ 0.1 kcal/mol free energy change between the two stationary points. There are several other rotamers of TME^+ , and **10** is a transition state for the internal rotation path that transforms **2** into a **2'** conformer with $\text{ca } -10^\circ$ torsion. The most stable TME^+ structure is, however, found at 90° . But this internal rotation shows more complexity than expected, and it proved difficult to locate a transition state between **2** and **3**. Therefore an internal rotation path was calculated by a torsion angle scan, between 0° (**10**) and 90° (**3**), where all other coordinates were optimized with B3LYP/6-31G(d,p) and subsequently a CCSD(T)/cc-pVDZ single point. The abrupt change in symmetry of the

HOMO at $\sim 42^\circ$ further supports that two different states are involved in this torsional mode.

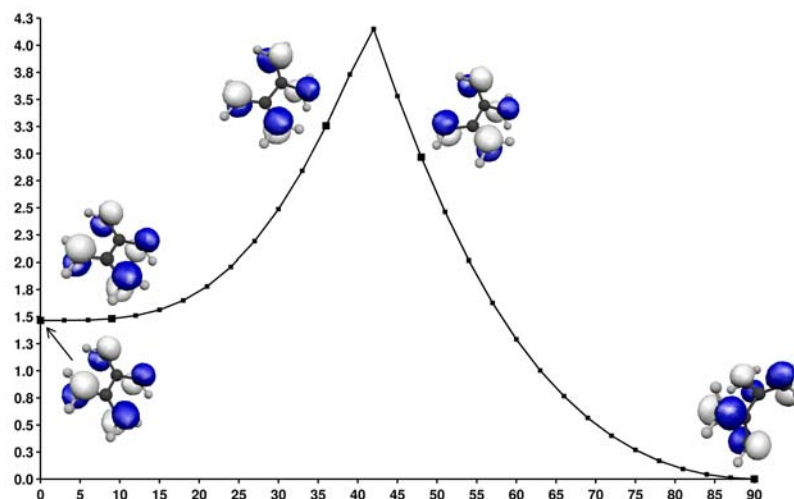


Figure 9. TME^+ internal rotation from 0° to 90° . The energies are from CCSD(T)/cc-pVDZ calculations on B3LYP/6-31G(d,p) optimized geometries. The HOMO of some selected conformers along the torsion is also shown, note the change in orbital symmetry at the cusp.

Rehybridization Mechanism

In both ring openings of BCP^+ a pyramidalization of C1 and C1' is the major coordinate involved in the mechanism. To investigate how rehybridization C2–C3 compares with bond breaking in the ring opening of the first cyclopropane ring (C1C2C3), bond breaking and pyramidalization are compared along the reaction path **1** to **5** (see Figure 10). An examination of this figure shows that the rehybridization is dominating over the C2–C3 bond breaking up to the intermediate point **i2**, and after **i2** the ring opening becomes dominating.

Moreover, using NBO calculations for **1**, **i1**, **i2** and **5** the proposed rehybridization mechanism can be justified. The NBO's for $\sigma_{\text{C2-C3}}$, n_1 and n_1' provide extra support for the importance of pyramidalization during the ring opening. Between **1** and **i2** the $\sigma_{\text{C2-C3}}$ is only slightly affected, with equivalent α and β NBOs throughout. That is, in **1**, $\alpha\text{-}\sigma_{\text{C2-C3}}$ is $0.707(\text{sp}^{3.33})_{\text{C2}} + 0.707(\text{sp}^{3.33})_{\text{C3}}$ with α and β occupations of 0.978e and 0.977e, respectively; while in **i2** $\alpha\text{-}\sigma_{\text{C2-C3}}$ is $0.699(\text{sp}^{4.97})_{\text{C2}} + 0.715(\text{sp}^{4.92})_{\text{C3}}$ with α and β occupations of 0.957e and 0.908e, respectively. The situation is different in **5**, where the natural hybrids show larger p-character, i.e., the α -

σ_{C2-C3} is $0.702(sp^{11.52})_{C2} + 0.712(sp^{11.58})_{C3}$ with α and β occupations of 0.922e and 0.723e, respectively, indicates a partly broken bond. Furthermore, n_1 increases its occupation along the reaction path from 0.207e in **1** to 0.210e in **i1** and further to 0.212e in **i2** and 0.341e in **5** while the occupation of n_1' decreases from 0.207e in **1** and **i1**, through 0.142e in **i2** to 0.136e in **5**. Hence, the NBO analysis shows that the rehybridization takes place without much change in electronic structure, and it is only after a finished rehybridization that a favourable structure for C2-C3 bond breaking is reached.

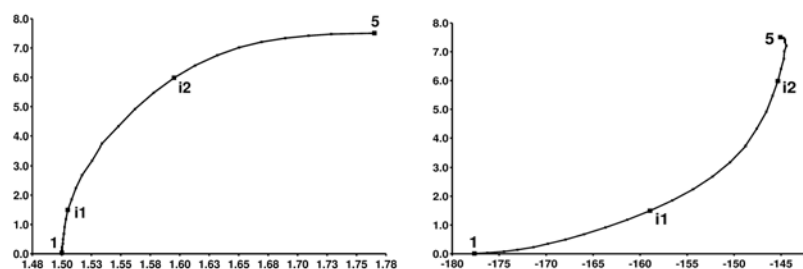


Figure 10. Reaction path from BCP^+ , **1**, to the rate-limiting transition structure, **5**. The B3LYP/6-31G(d,p) relative energy (kcal/mol) is plotted against the C2–C3 distance (Å) – left – and the variation of the C3C2C1C1'-dihedral angle (°) – right.

5. Principle of Least Motion

In a chemical reaction the nuclear coordinates evolve while the reaction path traverses the transition state and reaches the products. If it is assumed that the nuclear motion of this transformation is minimized, a simple model can be introduced that specifies the outcome of a chemical reaction by nuclear displacements, i.e., the principle of least motion (PLM). By a distance measure, the Rice-Teller measure based on hyperspherical coordinates, the PLM can be quantified; and, for example, applied to the highly complex rearrangement of the barbaralyl cation (Paper V).

A chemical reaction mechanism can also be described as an evolution of a reaction trajectory, tracing out the mechanism. This trajectory does then form a line in the nuclear coordinate space that links reactants with product molecules. Hence, if we follow the minimum energy path, RP, the change in nuclear coordinates describes the elementary reaction step that proceeds from the reactant geometry over a transition structure to products. A PLM model is invoked by an analogy with the idea of minimal action, and it is thus postulated that the nuclear displacement of a RP follows the path of least nuclear motion.

The principle of least action was introduced in physics by Pierre Louis Moreau de Maupertuis⁴⁹ and applied by Leonard Euler in ballistics, central force motion, etc. According to this principle, spontaneous movements are always associated with minimal changes in the quantity of action.⁵⁰ Later, during the construction of quantum mechanics a similar principle appeared, developed by de Broglie, Schwinger and Feynman, which also found some use in statistical mechanics.⁵¹

In chemistry, least motion ideas were first used by Muller who in 1886 introduced a rule of least molecular deformation in the course of chemical transformation.⁵² Since this idea was so appealing, it appeared in several textbooks as the principle of minimal structural change.⁵³ A more general formulation was done in 1936, called the principle of least motion, by Rice and Teller. As they formulated: a principle which states that there shall be least change in atomic position and least change in electronic configuration during an elementary reaction.⁵⁴ Their idea of a PLM implies that the constituent atoms of a molecular system must be displaced with respect to one another so that their nuclear motions are minimized. Besides the least

change in atomic motion, they also state that a change in electronic configuration should be minimal, which in a modern context could be interpreted as a least change in multiplicity, orbital symmetry, etc. Hence, according to Rice and Tellers PLM statement a reaction mechanism can be rationalized to consist of two effects: (a) least change in nuclear configuration; and (b) least change in electronic configuration. In the discussion here, the PLM will always refer to (a). Nevertheless, it is more common to use qualitative explanations that stems from part (b), and one obvious example is the orbital symmetry rules of Woodward and Hoffmann.

Yet, it may be worthwhile to investigate the use of PLM concepts as complementary simple models to those based on orbitals. However, to quantify the distance between different structures we need a measure. There are several different measures constructed for this purpose, most of them are based on the sum of the squares of the displacements,⁵⁵ of which, Ehrenson⁵⁶ has constructed the most rigorous that minimizes the sum of the squares of the mass-weighted Cartesian distortions

$$D_m^2 = \sum_{i=1}^N m_i d_i^2 = \sum_{i=1}^N m_i \left\{ (x'_i - x_i)^2 + (y'_i - y_i)^2 + (z'_i - z_i)^2 \right\} \quad (23)$$

where the primed coordinates refer to product and the unprimed to reactant. Actually, there exist many other types of measures and descriptors, for example, there have been several suggestions of measures for quantifying chirality;⁵⁷ or shape descriptors for analyzing molecular properties.⁵⁸ The use of a molecular measure to compare different elementary reaction steps based on PLM therefore seems entirely reasonable, and the PLM has indeed found some use in Organic Chemistry.^{55,59} But its main use is implicit, since mechanisms are often omitted by inspection, concluding that a particular geometrical change is regarded unlikely. Still, several types of organic reactions are thought to follow PLM paths, e.g., rearrangement, decomposition, and elimination type reactions.⁵⁵ The PLM has also been proposed as an alternative explanation for reactions governed by stereoelectronic control (SEC),⁵⁹ which is based on the effect that nonbonding electrons have on reactivity.⁶⁰ However, since SEC fails on several occasions, and involves the same type of frontier orbital explanations as the anomeric effect, the PLM is suggested to be a simpler and as valid way to interpret this type of reactions. Moreover, in enzyme and intramolecular reactivity, a similar idea – the proximity effect – has been proposed.⁶¹ Thus, it is the proximity of enzyme-substrate complexes that gives rise to the rate acceleration in enzymes. The suggestion is to replace entropy, which is a conglomerate of, for instance, changes in solvation

conformation, molecularity, etc., in enzyme reactivity with proximity. Hence, distance is proposed to be a more comprehensible quantity than entropy.

However, the PLM is a simplified model of chemical reactions and it will only capture the basic aspects of the actual nuclear motion involved in the chemical reaction. In experiments there are many complex interactions that are not included in any such simple model, that is, all dynamical effects, quantization of vibrations, rotations and electronic states are missing in a PLM description. A concept like PLM is therefore best regarded as a model that gives simple answers to otherwise complex transformations.¹

A. Rice-Teller Measure

The Rice-Teller measure developed by Linderberg⁶² is based on hyperspherical coordinates. The reason for using this type of coordinate system is that the internal coordinates can be separated into a size variable – the hyperradius – and directional coordinates in a kinematic space. As a result different combinations of the particles included in the system are mapped in specific directions in the multidimensional coordinate space.

A Rice-Teller measure is conveniently introduced from a quantum chemical calculation, where the different stationary points are given in Cartesian coordinates.⁶³ The hyperspherical coordinates are based on the ones used in atomic and molecular physics by Fano,⁶⁴ which Kupperman has applied to scattering theory.⁶⁵ If a stationary point on a PES is treated as a system of point masses, which are specified by the set of Cartesian coordinates $\{\mathbf{r}_j\}$ and mass values $\{m_j\}$, then for a suitable reference frame

$$\{(\mathbf{r}_j; m_j) \mid \mathbf{r}_j \in R^3, j = 1, 2, \dots, N\} \quad (24)$$

and denoting the total mass of the system with M

$$M = \sum_{j=1}^N m_j \quad (25)$$

and solving the variational problem

$$q = \min \sqrt{\left(\sum_{j=1}^N \frac{|\mathbf{r}_j - \mathbf{g}|^2 m_j}{M} \right)}; \quad \forall \mathbf{g} \in R^3 \quad (26)$$

The smallest value of q is the hyperradius, a measure of the size of the system, which is translationally and rotationally invariant,⁶⁶ and the vector \mathbf{g} is defining the centre of mass.

To measure distances between different conformations of the same molecular system, we need at least two distinct conformations that are defined by two sets of coordinates

$$\{(\mathbf{r}_{sj}; m_j) \mid \mathbf{r}_{sj} \in R^3, j = 1, 2, \dots, N, s = a, b\} \quad (27)$$

where each conformation is in its own reference frame. The distance between them is defined as the minimum value of a variational form

$$d_{ab} = \min \sqrt{\left[\sum_{j=1}^N \frac{|\mathbf{r}_{aj} - \mathbf{g}_a - \Omega_{ab}(\mathbf{r}_{bj} - \mathbf{g}_b)|^2 m_j}{M} \right]} \quad (28)$$

$$\forall \mathbf{g}_s \in R^3, s = a, b; \Omega_{ab} \in SO(3)$$

where only proper rotations are considered. This is a form invariant to translations and rotations of the reference frame. The optimal value for \mathbf{g}_a and \mathbf{g}_b is the center of mass. Moreover, the optimal rotation, Ω_{ab} , is established, if the reference frames are chosen such that the center of mass, \mathbf{g}_a and \mathbf{g}_b , equals zero, by using the condition that the distance d_{ab} is stationary with respect to infinitesimal rotations, which leads to the equation

$$\sum_{j=1}^N \frac{\partial \Omega_{ab} \mathbf{r}_{bj} \cdot \mathbf{r}_{aj} m_j}{M} = 0; \quad \Omega_{ab} \in SO(3) \quad (29)$$

For the representation of the $SO(3)$ elements the Euler-Rodrigues parameters are chosen⁶⁷

$$\Omega_{ab} \mathbf{r}_{bj} = \begin{bmatrix} \alpha_0^2 + \alpha_1^2 - \alpha_2^2 - \alpha_3^2 & 2\alpha_1\alpha_2 - 2\alpha_0\alpha_3 \\ 2\alpha_2\alpha_1 + 2\alpha_0\alpha_3 & \alpha_0^2 - \alpha_1^2 + \alpha_2^2 - \alpha_3^2 \\ 2\alpha_3\alpha_1 - 2\alpha_0\alpha_2 & 2\alpha_3\alpha_2 + 2\alpha_0\alpha_1 \end{bmatrix} \begin{bmatrix} x_{bj} \\ y_{bj} \\ z_{bj} \end{bmatrix}$$

$$1 = \alpha_0^2 + \alpha_1^2 + \alpha_2^2 + \alpha_3^2 \quad (30)$$

This representation leads to the form of a scalar product expressed as

$$S_{ab} = \sum_{j=1}^N \frac{\Omega_{ab} \mathbf{r}_{bj} \cdot \mathbf{r}_{aj} m_j}{M} = (\alpha_0^2 - \alpha_1^2 - \alpha_2^2 - \alpha_3^2) \sum_{j=1}^N \frac{\mathbf{r}_{bj} \cdot \mathbf{r}_{aj} m_j}{M}$$

$$+ 2 \sum_{j=1}^N \frac{(\mathbf{a} \cdot \mathbf{r}_{bj})(\mathbf{a} \cdot \mathbf{r}_{aj}) m_j}{M} + 2\alpha_0 \sum_{j=1}^N \frac{\mathbf{a}(\mathbf{r}_{bj} \times \mathbf{r}_{aj}) m_j}{M}$$

$$\mathbf{a} = (\alpha_1, \alpha_2, \alpha_3) \quad (31)$$

which is a symmetric quadratic form. Its maximum value, taking the constraint into account, is found from the eigenvalue problem

$$S_{ab} \alpha_0 = \alpha_0 \sum_{j=1}^N \frac{\mathbf{r}_{bj} \cdot \mathbf{r}_{aj} m_j}{M} + \sum_{j=1}^N \frac{\mathbf{a}(\mathbf{r}_{bj} \times \mathbf{r}_{aj}) m_j}{M}$$

$$S_{ab} \mathbf{a} = \alpha_0 \sum_{j=1}^N \frac{(\mathbf{r}_{bj} \times \mathbf{r}_{aj}) m_j}{M} - \mathbf{a} \sum_{j=1}^N \frac{\mathbf{r}_{bj} \cdot \mathbf{r}_{aj} m_j}{M}$$

$$+ \sum_{j=1}^N \frac{[\mathbf{r}_{bj}(\mathbf{a} \cdot \mathbf{r}_{aj}) + \mathbf{r}_{aj}(\mathbf{a} \cdot \mathbf{r}_{bj})] m_j}{M} \quad (32)$$

Using (18), (19) and (20) the distance between two conformations (16) is given as

$$d_{ab} = \sqrt{(q_a^2 - 2S_{ab} + q_b^2)} \quad (33)$$

The eigenvalue problem for the scalar product demonstrates that

$$S_{ab} \leq q_a q_b \quad (34)$$

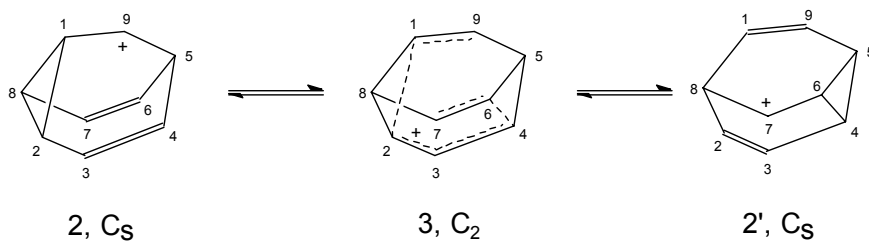
and an angular displacement can be defined

$$\omega_{ab} = \arccos \left[\frac{q_a^2 + q_b^2 - d_{ab}^2}{2q_a q_b} \right] \quad (35)$$

This angular relation is a measure in the $3N-6$ conformational space, based on hyperspherical coordinates, between two conformations. That is, a measure of the difference between two vectors in a many-dimensional coordinate space. The PLM is therefore measured as the angles between different conformations in this multidimensional coordinate space.

B. An Example: the Barbaralyl Cation

The barbaralyl cation, $C_9H_9^+$, has a 49-dimensional PES. Large areas of this space give no information about the barbaralyl cation, although other structures of interest exist.⁶⁸ Therefore selecting the area of the PES that needs special attention is vital, and the exploration of the region around the barbaralyl cation by Cremer et al⁶⁹ shows that the barbaralyl cation is a fluxional molecule that undergoes degenerate rearrangements. The Rice – Teller measure was used for this rearrangement reaction to see if it follows PLM trends.



Barbaralyl is a nonrigid molecule that undergoes a concerted reaction from **2** to **2'**. Yet, this mechanism is more intricate than the concerted transformation implies, since the activation barrier is very low for both this concerted partially degenerate rearrangement and also for the totally degenerate rearrangement.⁶⁹ The reaction mechanism for barbaralyl is better explained in Figure 11, where 11(a) shows the structures involved, and 11(b) a schematic description of the connections and a sketch of the PES, which forms a spider network of RPs instead of one single path. Two different types of paths can be separated as being of importance: first, a sixfold degenerate rearrangement cycle (the A1-A7 cycles in Figure 11); and second, the path that transforms in between the different A cycles (the B1-B6 cycles in Figure 11). The B path proceeds via a double bifurcation-path that connects three transition structures (the bold line in Figure 11(b)), moving from a transition structure in one A cycle over into a transition structure in another A cycle.

If the Rice-Teller measure (23) is applied to the barbaralyl reaction mechanism the six equilibrium structures **2**, C_s , distorted away from **1**, D_{3h} , have the angles shown in Table 1 with respect to each other. The labels are based on permutations of particles that are elements in a subgroup of the

Table 1. Distances between all six C_s equilibrium structures in one A-cycle.

g	a, a ²	b	ba, ba ²
ω_{ab}	13.25°	12.74°	10.41°

symmetric group S_9 .⁷⁰ Moreover, these structures have a common angular distance from the D_{3h} structure of 7.92°, and a hyperradius for D_{3h} that is 1.663 bohr, to be compared with the six C_s minima that have 1.706 bohr. In the hyperspherical coordinates the six C_s structures span a six-dimensional subspace, with the D_{3h} spanning a seventh, of the reduced 48 dimensional space of the barbaralyl cation; and the angles measure how close the next conformation is in this space.

Between two neighbouring equilibrium structures C_s , one transition structure C_2 and a bifurcation transition structure C_{2v} are located. Both should be displaced from C_s with a small angle, and indeed the C_2 is 6.43° from the closest two C_s , and the C_{2v} is located only 8.95° away. Yet, the closest distance is between the two transition structures, C_2 and C_{2v} , of 4.22°. In Table 2 many other angular distances are presented, and Figure 12 shows a scheme over the relative locations in this space.

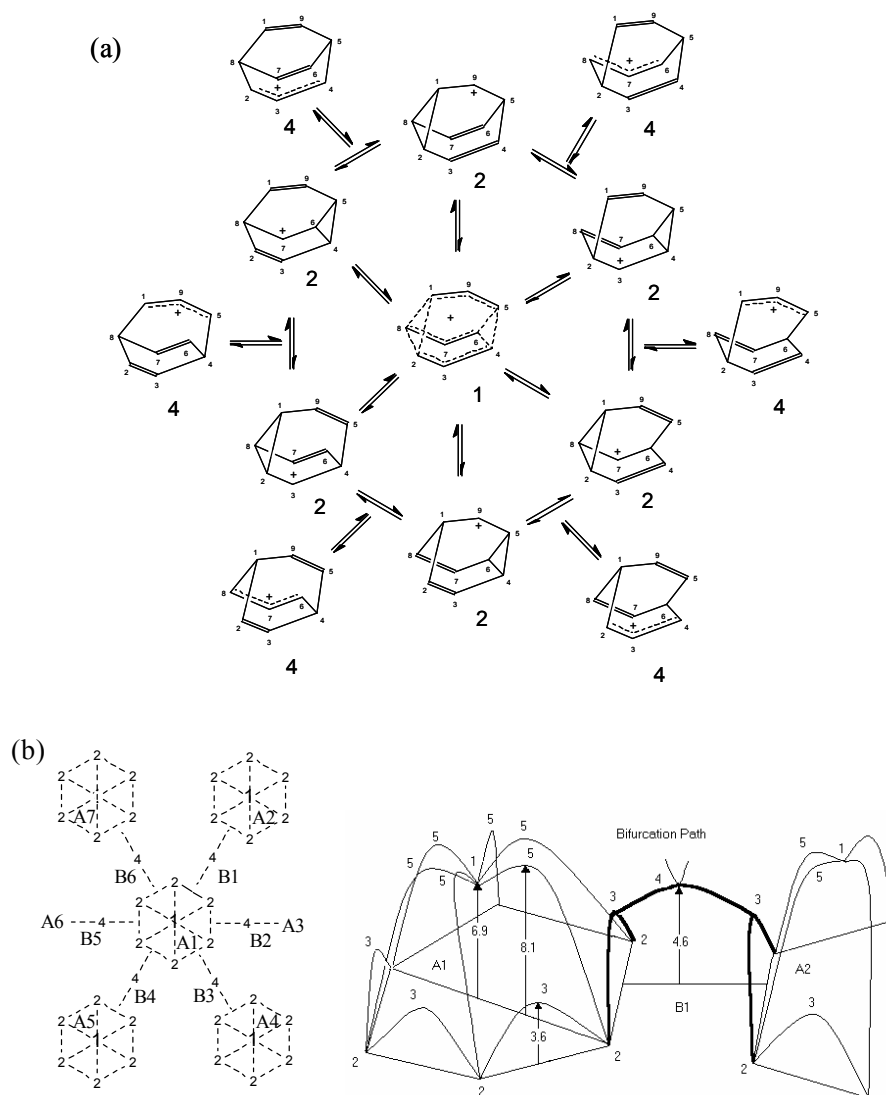


Figure 11. The rearrangement mechanism for the barbaralyl cation. In (a) the sixfold rearrangement cycle A1, for which the six degenerate **2** are connected with the D_{3h} symmetrical ion **1** in the center of the cycle. Moreover, each A1-cycle is connected with six other cycles (A2-A7) via **4**. In (b) left, the connections between the different A-cycles through the B1-B6 processes, where the dashed lines indicate the reaction paths connecting different species. In (b) right, the barrier heights for the different rearrangements, where the bold lines indicate the bifurcation path of B1 leading from cycle A1 to A2 with structure **4** as transition structure. The barrier heights are taken from MP4(SDQ)/6-31G(d) calculations and are given in kcal/mol (adapted from ref. 69.).

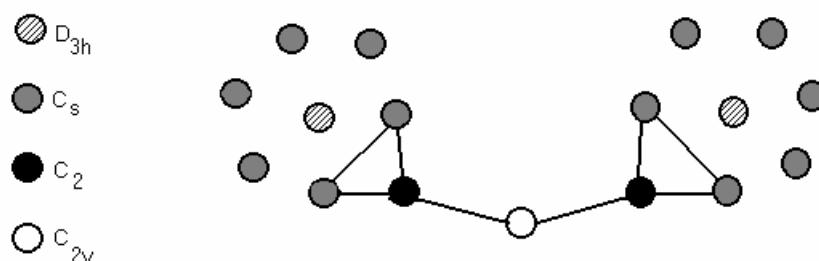


Figure 12. The relative positions for two rearrangement cycles, i.e., the C_s -equilibrium geometries (2), a C_2 -TS (3), a C_{2v} -bifurcation-TS (4) connecting both C_2 -TS, and the corresponding two D_{3h} (1) for each cycle. Note that the distances only approximately reflect the ones from Table 2 (adapted from ref. 70).

Table 2. Angular distances for the four structures presented in Figure 12.

	D_{3h}	C_s	C_s	C_s	C_s	C_s	C_s	C_2	C_{2v}
C_s	7.92								
C_s	7.92	10.41							
C_s	7.92	10.41	13.25						
C_s	7.92	13.25	10.41	12.74					
C_s	7.92	12.74	13.25	13.25	10.41				
C_s	7.92	13.25	12.74	10.41	13.25	10.41			
C_2	9.59	14.65	14.65	13.71	13.71	6.43	6.43		
C_{2v}	12.93	17.80	17.80	16.36	16.36	8.95	8.95	4.22	
C_2	15.93	20.60	20.60	18.71	18.71	11.91	11.91	8.16	4.22
C_s	18.35	22.20	23.50	20.59	20.82	14.30	15.23	11.91	8.95
C_s	18.35	23.50	22.20	20.82	20.59	15.23	14.30	11.91	8.95
C_s	23.72	27.41	28.57	25.19	25.55	20.82	20.59	18.71	16.36
C_s	23.72	28.57	27.41	25.55	25.19	20.59	20.82	18.71	16.36
C_s	26.02	29.80	28.66	28.57	27.41	22.20	23.50	20.60	17.80
C_s	26.02	28.66	29.80	27.41	28.57	23.50	22.20	20.60	17.80
D_{3h}	21.76	26.02	26.02	23.72	23.72	18.35	18.35	15.93	12.93

In conclusion, the Rice-Teller measure for estimating differences between conformations on a PES, does indeed order the conformations according to the PLM for the barbaralyl cation. That is, it arranges the conformations in proper order, with the smallest angles being closest on the RP. A successful result for such a complex rearrangement is encouraging, and may imply that the PLM is more general than previously thought when simpler measures were employed. However, for a hyperspherical coordinate the barbaralyl

cation is almost the best scenario, because all C_s minima, all C_2 transition structures, etc. have the same geometry for its different stationary points, respectively, and it is only the labels of the atoms that change. Thus, all C_s conformations have the same hyperradius, and the distance between them is just the angular transformation on a hypersphere. The same is true for the other conformations but with their own specific hyperspheres. For those chemical reactions that have large structural alterations in a reactive event, it is probably not as beneficial to use an angular measure. Nevertheless, for the barbaralyl cation a transformation into hyperspherical coordinates result in a conclusion that its complex RPs follows the PLM; and this result may imply that a PLM can be recovered in a more general scale, if the proper coordinate transformation is applied.

Acknowledgment

In writing this short text about modelling chemical reactions with quantum chemical methods, several friends and teachers have provided invaluable help, advice, patience and, not least, put out some obstacles to be conquered. Particular thanks are due to all my teachers; of special importance for this work are: Dr Nessima Salhi-Benachenhou, for reading and correcting this and several other manuscripts and all support; Prof Sten Lunell, for all radical quantum chemistry knowledge; Prof Olle Matsson, for all help with organic chemistry; Prof Osvaldo Goscinski, for sharing his chemical physics and physics knowledge and all jokes; and Prof Jan Linderberg, for trying to teach a hopeless case like me how to find the least motion path and for the hospitality during my stay in Århus.

I've also been blessed with some lovely (in)mates at the quantum chemistry group during my stay. I'm particularly grateful for all help given by Maria Lundqvist and, indeed, Jorge Llano to finish this text. Finally, since I'm just to be released, I must also send shout outs to all past and present members of the quantum chemistry group and all my other friends, and I'm out, peace for 2003.

References

1. Hoffmann, R.; Minkin, V. I.; Carpenter, B. K. *Bull. Soc. Chim. Fr.* **133**, 117 (1996).
2. Segal, L. A. *Complexity* **1**, 18 (1995).
3. Ceperley, D. M. *Rev. Mod. Phys.* **71**, S438 (1999).
4. Oreskes, N.; Shrader-Frechette, K.; Belitz, K. *Science* **263**, 641 (1994).
5. Cartwright, N. *How the laws of physics lie* (Clarendon Press, Oxford, UK, 1983).
6. (a) Maksic, Z. B. In *Theoretical Models of Chemical Bonding. Part 1: Atomic Hypothesis and the concept of Molecular Structure*; Maksic, Z. B., ed. (Springer-Verlag, Berlin, Germany, 1990);
(b) Tomasi, J. J. *Mol. Struct. (THEOCHEM)* **179**, 273 (1988);
(c) Trindle, C. *Croatia Chem. Acta* **57**, 1231 (1984);
(d) Bhushan, N.; Rosenfeld, S. J. *Chem. Educ.* **72**, 578 (1995).
7. (a) Primas, H. *Chemistry, Quantum mechanics and reductionism* (Springer, Berlin, Germany, 1983);
(b) Anderson, P. W. *Science* **177**, 393 (1972);
(c) Weinberg, S. *Nature* **330**, 443 (1987);
(d) Mayr, E. *Nature* **331**, 475 (1988);
(e) Theobald, D. W. *Chem. Soc. Rev.* **5**, 203 (1976);
(f) Ramsey, J. L. In *Conceptual perspectives in Quantum Chemistry*; Calais, J.-L. and Kryachko, E., eds. (Kluwer Acad. Publ., Dordrecht, Netherlands, 1997);
(g) Laughlin, R. B.; Pines, D. *PNAS* **97**, 28 (2000).
8. London, F. Z. *Elektrochemie* **35**, 552 (1929).
9. Eyring, H.; Polanyi, M. *Z. Phys. Chem. B* **12**, 279 (1931).
10. Born, M.; Oppenheimer, J. R. *Ann. Physik* **84**, 457 (1927).

11. Born, M.; Huang, K. *Dynamical theory of Crystal Lattices* (Oxford University Press, Oxford, UK, 1955).
12. Fukui, K. *Acc. Chem. Res.* **14**, 363 (1981).
13. Heidrich, D. In *The Reaction Path in Chemistry: Current approaches and perspectives*; Heidrich, D., ed. (Kluwer Acad. Publ., Dordrecht, Netherlands, 1995).
14. (a) Ayala, P. Y.; Schlegel, H. B. *J. Chem. Phys.* **107**, 375 (1997);
 (b) Elber, R.; Karplus, M. *Chem. Phys. Lett.* **139**, 375 (1987);
 (c) Jasien, P. G.; Shepard, R. *Int. J. Quant. Chem., Quant. Symp.* **22**, 183 (1988);
 (d) Stacho, L. L.; Ban, M. I. *Theor. Chim. Acta* **83**, 433 (1992);
 (e) Chiu, S. S.-L.; McDouall, J. J. W.; Hillier, I. H. *J. Chem. Soc. Faraday Trans.* **90**, 1575 (1994);
 (f) Passerone, D.; Parrinello, M. *Phys. Rev. Lett.* **87**, 108302 (2001).
15. Surface constructed from equations given by Schlegel, H. B. In *Modern Electronic Structure Theory*; Yarkony, D. R., ed. (World Scientific, Singapore, 1995).
16. (a) Moore, J. W.; Pearson, R. G. *Kinetics and Mechanism* (Wiley, New York, USA, 1981);
 (b) Laidler, K. J. *Chemical Kinetics* (Harper&Row, Hilversum, Netherlands, 1987);
 (c) Steinfeld, J. I.; Francisco, J. S. and Hase, W. L. *Chemical Kinetics and Dynamics* (Prentice Hall, Upper Saddle River, USA, 1999);
 (d) Hammett, L. P. *Physical Organic Chemistry: Reaction Rates, Equilibria, and Mechanism* (McGraw-Hill, New York, USA, 1970).
17. Kreevoy, M. M.; Truhlar, D. G. In *Investigation of Rates and Mechanisms of Reactions, Part I*; Bernasconi, C. F., ed. (Wiley, New York, USA, 1986).
18. (a) Williams, I. H. *Chem. Soc. Rev.* **22**, 277 (1993);
 (b) Wiest, O.; Montiel, D. C.; Houk, K. N. *J. Phys. Chem. A* **101**, 8378 (1997).
19. Doubleday, C.; McIver, J.; Page, M.; Zielinski, T. J. *Am. Chem. Soc.* **107**, 5800 (1985).
20. Truhlar, D. G.; Isaacson, A. D.; Garret, B. C. In *Theory of Chemical Reaction Dynamics*; Baer, M., ed. (CRC Press, Boca Raton, FL, USA, 1985).
21. For more general overviews several excellent books are available. Two examples are:

- (a) Cramer, C. J. *Essentials of Computational Chemistry: Theories and Models* (John Wiley, Chichester, U.K., 2002);
- (b) Jensen, F. *Introduction to Computational Chemistry* (John Wiley, Chichester, U.K., 1999).
22. Sutcliffe, B. T. In *Computational Techniques in Quantum Chemistry and Molecular Physics*; Dierksen, G. H. F.; Sutcliffe, B. T.; Veillard, A., eds. (Reidel, Dordrecht, Netherlands, 1975)
23. (a) Szabo, A.; Ostlund, N. *Modern Quantum Chemistry* (McGraw-Hill, New York, USA, 1989);
- (b) McWeeny, R. *Methods of Molecular Quantum Mechanics* (Academic Press, London, U.K., 1992);
- (c) Helgaker, T.; Jorgensen, P.; Olsen, J. *Electronic Structure Theory* (Wiley, New York, USA, 1999).
24. (a) Parr, R. G.; Yang, W. *Density Functional Theory of Atoms and Molecules* (Oxford U. P., New York, USA, 1989);
- (b) Koch, W.; Holthausen, M. C. *A Chemist's Guide to Density Functional Theory* (Wiley-VCH, Weinheim, Germany, 2001).
25. Head-Gordon, M. J. *Phys. Chem.* **100**, 13213 (1996).
26. Raghavachari, K.; Trucks, G. W.; Pople, J. A.; Head-Gordon, M. *Chem. Phys. Lett.* **157**, 479 (1989).
27. Becke, A. D. In *Modern Electronic Structure Theory Vol. 2*; Yarkony, D. R. ed. (World Scientific, Singapore, 1995).
28. (a) Davidson, E. R.; Feller, D. *Chem. Rev.* **86**, 681 (1986);
- (b) Shavitt, I. *Isr. J. Chem.* **33**, 357 (1993).
29. Weil, J. A.; Wertz, J. E.; Bolton, J. R. *Electron Paramagnetic Resonance* (Wiley, New York, USA, 1994).
30. Karplus, M.; Porter, R. N. *Atoms and Molecules* (Benjamin/Cummings, New York, USA, 1970).
31. Feller, D.; Davidson, E. R. *J. Chem. Phys.* **88**, 7580 (1988).
32. (a) Barone, V. In: *Recent Advances in Density Functional Methods*, Chong, D. P. ed. (World Scientific, Singapore, 1995);
- (b) O'Malley, P. J. *J. Phys. Chem. A* **101**, 6334 (1997);
- (c) Batra, R.; Giese, B.; Spichty, M.; Gescheidt, G.; Houk, K. N. *J. Phys. Chem.* **100**, 18371 (1996).
33. Schmittel, M.; Burghart, A. *Angew. Chem. Int. Ed. Engl.* **36**, 2550 (1997).

34. Roth, H. D. *Top. Curr. Chem.* **163**, 131 (1992).
35. Ishiguro, K.; Khudyakov, I. V.; McGarry, P. F.; Turro, N. F.; Roth, H. D. *J. Am. Chem. Soc.* **116**, 6933 (1994).
36. Cromack, K. R.; Werst, D. W.; Barnabas, M. V.; Trifunac, A. D. *Chem. Phys. Lett.* **218**, 485 (1994).
37. (a) Clark, T. *Acta Chem. Scand.* **51**, 646 (1997);
(b) Inadomi, Y.; Morihashi, K.; Kikuchi, O. *J. Mol. Struct. (Theochem)* **434**, 59 (1998);
(c) Bach, R.D.; Schilke, I. L.; Schlegel, H. B. *J. Org. Chem.* **61**, 4845 (1996);
(d) Raghavachari, K.; Haddon, R. C.; Roth, H. D. *J. Am. Chem. Soc.* **105**, 3110 (1983).
38. Chen, G.-F.; Wang, J. T.; Williams, F.; Belfield, K. D.; Baldwin, J. E. *J. Am. Chem. Soc.* **113**, 9853 (1991).
39. Barnabas, M. V.; Werst, D. W.; Trifunac, A. D. *Chem. Phys. Lett.* **206**, 21 (1993).
40. Bühler, R. E.; Quadir, M. A. *J. Phys. Chem. A* **104**, 2634 (2000).
41. Adam, W.; Heidenfelder, T.; Sahin C. *J. Am. Chem. Soc.* **117**, 9693 (1995).
42. Herges, R.; Starck, F.; Winkler, T.; Schmittel, M. *Chem. Eur. J.* **5**, 2965 (1999).
43. Faucitano, A.; Buttafava, A.; Martinotti, F.; Sustmann, R. *J. Chem. Soc. Perkin Trans.* **2**, 865 (1992).
44. (a) Laube, T. *Acc. Chem. Res.* **28**, 399 (1995) and references therein;
(b) Schleyer, P. v. R.; Maerker, C. *Pure & Appl. Chem.* **67**, 755 (1995), and references therein;
(c) Bremer, M.; Schötz, K.; Schleyer, P. v. R.; Fleischer, U.; Schindler, M.; Kutzelnigg, W.; Koch, W.; Pulay, P. *Angew. Chem. Int. Ed. Engl.* **28**, 1042 (1989).
45. (a) Hirano, T.; Shiina, S.; Ohashi, M. *J. Chem. Soc., Chem. Commun.* 1544 (1992);
(b) Ishii, H.; Shiina, S.; Hirano, T.; Niwa, H.; Ohashi, M. *Tetrahedron Lett.* 523 (1999);
(c) Roth, H. D.; Du, X.-M.; Weng, H.; Lakkaraju, P. S.; Abelt, C. J. *J. Am. Chem. Soc.* **116**, 7744 (1994);
(d) Abelt, C. J.; Roth, H. D. *J. Am. Chem. Soc.* **108**, 6734 (1986);
(e) Roth, H. D. *Adv. Theoret. Interest. Mol.* **3**, 261 (1995).

46. See, for instance, the thematic issue on cyclopropane chemistry in *Chem. Rev.* **103** (4), (2003).
47. (a) Gerson, F.; de Meijere, A.; Qin, X.-Z. *J. Am. Chem. Soc.* **111**, 1135 (1989);
(b) Gerson, F.; Schmidlin, R.; de Meijere, A.; Späth, T. *J. Am. Chem. Soc.* **117**, 8431 (1995).
48. Salhi-Benachenhou, N.; Engels, B.; Huang, M.-B.; Lunell, S. *Chem. Phys.* **236**, 53 (1998). See also references therein.
49. Maupertuis, P. L. M. *Mémoires de l'Académie Royale* 423, (1744).
50. Feynman, R. P.; Leighton, R. B.; Sands, M. *The Feynman Lectures on Physics Vol. 2* (Addison-Wesley, Reading, USA, 1989).
51. Feynman, R. P.; Hibbs, A. R. *Quantum Mechanics and Path Integrals* (McGraw-Hill, New York, USA, 1965).
52. Muller, A. *Bull. Soc. Chim. Fr.* **45**, 438 (1886).
53. (a) Hückel, W. *Theoretische Grundlagen der Organischen Chemie* (Akademische Verlagsgesellschaft, Leipzig, Germany, 1934);
(b) Wheland, G. W. *Advanced Organic Chemistry* (Wiley, New York, USA, 1960).
54. Rice, F.; Teller, E. *J. Chem. Phys.* **6**, 489 (1936).
55. Hine, J. *Adv. Phys. Org. Chem.* **15**, 1 (1977).
56. Ehrenson, S. *J. Am. Chem. Soc.* **96**, 3778; 3784 (1974).
57. Buda, A. B.; Auf der Heyde, T.; Mislow, K. *Angew. Chem. Int. Ed. Engl.* **31**, 989 (1992).
58. (a) Mezey, P. G. *Shape in Chemistry: An Introduction to Molecular Shape and Topology* (VCH, New York, USA, 1993);
(b) Arteca, G. A. In *Rev. Comp. Chem. Vol. 9*; Lipkowitz, K. B. and Boyd, D. B., eds. (VCH, New York, USA, 1996).
59. Sinnott, M. L. *Adv. Phys. Org. Chem.* **24**, 113 (1988).
60. Kirby, A. J. *Stereoelectronic Effects* (Oxford University Press, Oxford, UK, 1996).
61. Menger, F. M. *Acc. Chem. Res.* **26**, 206 (1993).
62. Linderberg, J. In *New Methods in Quantum theory*; Tsipis et al., eds. (Kluwer Acad. Publ., Dordrecht, Netherlands, 1996).
63. Linderberg, J. *J. Chem. Soc., Faraday Trans.* **93**, 893 (1997).
64. Fano, U. *Phys. Rev. A* **24**, 2402 (1981).

65. Kupperman, A.; Kaye, J. A.; Dwyer, J. P. *Chem. Phys. Lett.* **74**, 257 (1980).
66. (a) Öhrn, Y.; Linderberg, J. *Mol. Phys.* **49**, 53 (1983);
(b) Smith, F. T. *Phys. Rev.* **120**, 1058 (1960).
67. Biedenharn, L. C.; Louck, J. D. *Angular Momentum in Quantum Physics* (Addison-Wesley, Reading, UK, 1980).
68. Ahlberg, P.; Jonsäll, G.; Engdahl, C. *Adv. Phys. Org. Chem.* **19**, 223 (1983).
69. Cremer, D.; Svensson, P.; Kraka, E.; Ahlberg, P. *J. Am. Chem. Soc.* **115**, 7445 (1993).
70. Larsson, P.-E.; Linderberg, J. *Theor. Chim. Acta* **93**, 79 (1996).